Using delta channel width to estimate paleodischarge in the rock record: geometric scaling and practical sampling criteria

O.A. Prasojo[1,2*], A. E. van Yperen[3], T. B. Hoey[4], A. Owen[1] and R. Williams[1]

[1]School of Geographical and Earth Sciences, University of Glasgow, University Avenue, Glasgow, G12 8NN, United Kingdom, octria.prasojo@glasgow.ac.uk, Amanda.Owen@glasgow.ac.uk, Richard.Williams@glasgow.ac.uk

[2]Geoscience Study Program, Faculty of Mathematics and Natural Sciences (FMIPA), Universitas Indonesia, Depok 16424, Indonesia.

[3]Department of Geosciences, University of Oslo, 0316 Oslo, Norway, annavanyperen@gmail.com

[4]Department of Civil and Environmental Engineering, Brunel University London, Uxbridge, UB8 3PH, United Kingdom, Trevor.Hoey@brunel.ac.uk

ABSTRACT

Quantifying paleodischarge from geological field observations remains a key research challenge. Several scaling relationships between paleodischarge and channel morphology (width; depth) have been developed for rivers and river deltas. Previous paleodischarge scaling relationships were based on discharge-catchment area scaling and an empirical flow velocity estimate (e.g. Chézy, Manning formulae) multiplied by channel cross-sectional area to derive discharge. In deltas, where marine (wave, tide) energy causes bidirectional flow within distributary channels, the available paleodischarge scaling relationships are not applicable due to their unidirectional flow assumption. Here, the spatial variability of distributary channel widths from a database of 114 global modern river deltas is assessed to understand the limit of marine influence on distributary channel widths. Using 6213 distributary channel width measurements, the median

channel widths of distributary channels for each delta were correlated with bankfull discharge for river-, tide- and wave-dominated deltas, the latter two including the effect of bidirectional flow. Statistically significant width-discharge scaling relationships are derived for river- and wave-dominated deltas, with no significant relationships identified for tide-dominated deltas. By reverse bootstrapping the channel widths measured from modern deltas, the minimum number of width measurements needed to apply width-discharge scaling relationships to ancient deltaic deposits is estimated as 3 and 4 for the upstream parts of river- and wave-dominated deltas, respectively, increasing to 30 in the downstream parts of river-dominated deltas. These estimates will guide sedimentological studies that often have limited numbers of distributary channel widths exposed in the rock record. To test the reliability of these alternative width-discharge scaling relationships in the rock record, paleodischarges were estimated for the well-studied Cretaceous lower Mesa Rica Sandstone Formation, USA. Comparison of these results with the more complex Chézy-derived method suggests that these new scaling relationships are accurate. Hence, it is proposed that the scaling relationships obtained from modern deltas can be applied to the rock record, requiring fewer, and easier to measure, data inputs than previously published methods.

INTRODUCTION

Estimating paleodischarge for ancient deltaic sequences mainly stems from scaling relationships developed in river settings, in which flow is assumed to be unidirectional. However, applying available paleodischarge estimation from rivers to deltaic settings may be inappropriate due to deltas' different morphological and flow characteristics. Estimating total paleodischarge over a delta requires that all channels are sampled or, alternatively, that whole system discharge is related to the geometry of single channels. Further, as a delta interacts with a standing body of water, processes such as the backwater effect and wave and tidal action may induce bidirectional

flow, making calculations based on uni-directional flow regimes no longer appropriate (Besset et al., 2017). There is thus a need to assess whether existing paleodischarge estimation techniques are appropriate for application to deltas, and to derive paleodischarge estimation techniques that are based on single channels in multi-channel systems, and/or that apply to process environments associated with bi-directional flow.

Most of the models proposed to estimate river paleodischarge, such as discharge-catchment area scaling (Syvitski and Milliman, 2007; Davidson and North, 2009) and flow velocity-based equations (Holbrook and Wanas, 2014; Bhattacharya et al., 2016) exclude the influence of marine energies that may produce bidirectional flow and so influence channel morphology. The discharge-catchment area scaling model incorporates water discharge (Q) and catchment area (A) from the 63% of the world's river discharge ($Q = 0.075A^{0.8}$), assuming that these two variables are partly independent (Syvitski and Milliman, 2007). We refer to this discharge-catchment area scaling as a 'macro method' because this method uses whole catchment area to determine water discharge. Consequently, applying discharge-catchment area scaling to ancient sedimentary systems needs robust paleogeographic reconstructions to estimate the paleocatchment area, itself challenging to reconstruct from the rock record (Allen et al., 2013; Brewer et al., 2020; Lyster et al., 2020). An alternative approach, that we refer as 'micro methods', uses empirical roughness equations to estimate flow velocity from which discharge is determined by multiplying flow velocity by channel cross-sectional area (Parker, 2004). Similar to discharge-catchment area scaling, the flow velocity-based equations need measurements or estimates of several parameters that are challenging to extract from the rock record: bankfull depth and width, paleoslope, and roughness coefficient, and assumed bankfull Shield's stress if the channel geometry is fully preserved (Holbrook and Wanas, 2014; Bhattacharya et al., 2016; Brewer et al., 2020). If the channel

geometry is not fully preserved, grain size and/or bedform amplitude may be used to estimate bankfull channel depth. Moreover, applying flow velocity-based equations requires knowledge of the total number of distributary channels and their total cross-sectional area to estimate the total discharge to the delta, which is challenging data to obtain from the rock record due to the need for extensive outcrop or borehole coverage.

Recently, Prasojo et al. (2023) produced both global and climate-specific scaling relationships between bankfull water discharge (Q) and median distributary channel width (w) of 66 river-dominated deltas from modern system, as summarized in Table 1. Prasojo et al. (2023) used these new 'macro' relationships to produce paleodischarge estimates for two Cretaceous formations that were similar to those produced by both discharge-catchment area scaling and flow velocity equations. Both the global and climate-specific scaling relationships are statistically significant, with $p < 0.05$, $R^2 > 0.53$ and 95% confidence intervals of ± 52 m^3/s. These models effectively removed the role of tidal and wave processes that may alter the geometry of the distributary channels by using the median width measured across each delta. However, in wave or tide-dominated deltas, this median may be affected by marine processes which may consequently affect the statistical correlation between discharge and median distributary channel width determined before. Hence, equations that take account of marine processes are needed.

It is expected that scaling relationships between delta channel width and bankfull discharge weaken with increasing marine energy influence (wave, tide, longshore currents) due to bidirectional flow, hydraulic backwater effects and channel deflection in the more distal parts of delta plains (Besset et al., 2017). The influences of these downstream boundary conditions also significantly alter the geometry of delta distributary channels as has also been demonstrated (Fig. 1) (Chatanantavet et al., 2012; Lamb et al., 2012; Nittrouer, 2013; Fernandes et al., 2016; Ganti et

al., 2016; Martin et al., 2018; Gugliotta and Saito, 2019; Chadwick et al., 2019; Chadwick et al., 2020). Breakpoints in down-dip distributary channel morphology often represent the upstream limit of marine influences on channel widths (Sassi et al., 2012). The break in channel morphology can be defined as the location on the delta plain where distributary channel width starts to increase in contrast to the usual trend of constant or decreasing width downstream. This morphological boundary allows the delta plains of river-, tide- and wave-dominated deltas to be divided into upstream, assuming no marine influence, and downstream, marine-influenced parts. The downstream part is characterised by channels which widen towards the sea, whereas in the upstream part channel widths remain broadly constant between successive bifurcations to the delta apex. Using this differentiation, new equations can be developed for discharge or paleodischarge estimation from river deltas that are specific to delta type and so potentially provide greater confidence when used predictively than previously published models (Prasojo et al., 2023).

This study assesses the spatial variability of distributary channel widths from a database of 114 global river deltas to derive new channel width-discharge scaling relationships, in which a clear break in distributary channel widths is identified that separates upstream and downstream parts of the delta. A total of 6213 distributary channel widths from the 114 river deltas were measured from the delta apex, or first avulsion point, to the shoreline.

In contrast with modern river deltas, on which distributary channel widths can be measured directly from satellite imagery or in the field, ancient delta deposits typically have very limited distributary channel exposure or preservation hence the width cannot be determined directly. In this study we apply a reverse bootstrap method to the large global modern delta dataset (N = 6213) to estimate the optimum number of measurements needed to estimate paleodischarge from a rock record deltaic deposit.

Overall, the aims of this study are to: (1) separate upstream and downstream parts of deltas by identifying breaks along downstream (down-dip) direction of distributary channel widths; (2) derive new channel width-discharge scaling relationships for delta channels, separating data both between upstream and downstream parts of deltas, and dominant delta processes; (3) apply a reverse bootstrap method to the modern delta data to simulate the uncertainty in paleodischarge estimates from the limited number of data points usually available from the rock record; and, (4) compare the results from the new channel width-discharge scaling relationships with those obtained using a flow velocity-based equation for the Cenomanian lower Mesa Rica Sandstone (Dakota Group, USA).

METHODS

Deltas were identified based on protrusion of their subaerial deposits beyond their lateral shorelines with one or more distributary channels that are visible from satellite imagery (Bhattacharya, 2006; Caldwell et al., 2019). Deltas were then classified based on the relative dominance of river, wave or tide processes on their typical morphology. Morphologically, river-dominated deltas are characterized by one or more elongated distributary channels that protrude beyond the shoreline and subaerial mouth bar deposits (Olariu and Bhattacharya, 2006). Wave-dominated deltas have linear shorefaces and mouth bars modified by wave action. In most cases, wave-dominated deltas have a limited number of distributary channels (Bhattacharya and Giosan, 2003; Bhattacharya and Tye, 2004; Li et al., 2011). Tide-dominated deltas are characterized by funnel-shaped distributary channels with abundant tidal creeks on adjacent delta plains. We validated our morphological-based classification against Nienhuis et al.'s (2020) classification that used relative sediment fluxes. We simplify the classification into the three end-members of Galloway (1975), which is the same as Nienhuis et al. (2020), but acknowledge that other delta

138 classifications are available (Li et al., 2011; Vakarelov and Ainsworth, 2013; Lin and
139 Bhattacharya, 2021). The term 'dominated' is used in the delta classification to reflect the
140 dominant process (e.g. wave, tide, or river dominance) that affects distributary channels'
141 downstream geometry, as investigated in this study. Being classified into the wave-, tide-, or river-
142 dominated category does not imply that deltas are controlled by only wave, tide, or river processes
143 since almost no natural deltas falls entirely into any of these end members (Nienhuis et al., 2020).
144 Hence, the classification used in this study should be treated as relative dominance instead of a
145 discrete classification (Galloway, 1975; Nienhuis et al., 2020).

146 ***Dimensionless distributary channel widths of river deltas***

147 Wetted channel widths of distributary channels from 114 deltas (of which 97 are river-
148 dominated, 7 tide-dominated, and 10 wave-dominated) across different climate regions were
149 measured from annual composite Landsat 5 satellite imagery in ArcGIS (Fig. 2A). The earliest
150 (~1987) and the least cloudy images were chosen for image clarity purposes, as well as to minimize
151 the influence of ongoing anthropogenic activities such as embankment construction. Distributary
152 channel widths were measured manually along all the identifiable distributary channels seen on
153 annual composite 30-m resolution Landsat 5 from the delta apex to the shoreline. The delta apex
154 is assumed to be the present-day most landward bifurcation point observed on satellite images
155 (Ganti et al., 2016). Where deltas have a single channel, the delta apex is associated with the valley
156 exit point identified on a Digital Elevation Model (DEM) (Hartley et al., 2017). To enable
157 comparison of channel widths measured from different sized deltas, we use the semicircular grid
158 *s/L* method (Sassi et al., 2012) to ensure even spacing of measurements, where *s* represents the
159 along-channel distance from the delta apex, and *L* is the along-channel distance of the longest
160 distributary channel to the delta apex (Fig. 2B). Widths are measured as a straight line between the
161 two intersections between the semicircular grid and the riverbanks. The semicircular grid allows

measurement of multiple distributary channels located at the same dimensionless distance from the apex. The grid resolution is ~10 times the river channel width at the delta apex to maintain consistent dimensionless distance and data collection frequency across deltas of varying size. As an example, if a delta has a 100 m wide channel at its apex, the semicircular grid will have diameters of 1, 2, 3... km until the grid covers the entire delta plain (Fig. 2C). Thus, channel width is measured at s/L = 1, 0.9, 0.8... , 0.1, 0. Only channel widths (N = 6213) along definite distributary channels were included to exclude the influence of non-riverine channels, such as tidal creeks, in deltas. Consequently, only distributary channels that were be connected to the delta apex were measured in this study, to exclude tidal creeks. Where distributary channels contain mid-channel bars, the width of the whole channel was measured (Fig. 2D).

Dimensionless distance was plotted against dimensionless channel width (W^*) for each delta type. Dimensionless distance is defined as s/L consistent with the semicircular grid (Fig. 2B) that originates at the delta apex, and $W^* = W_i/W_A$ where W_i is channel width at location i and W_A is the channel width at the delta apex. Subsequently, downstream changes in dimensionless channel widths form the basis of classifying the delta plain into upstream and downstream parts. To identify the location of breakpoints in channel width-distance relationships between upstream and downstream regions, the non-parametric Kruskal-Wallis one-way analysis of variance test was used. Since the s/L method centralizes the avulsion length and apex channel width as the basis of creating the semicircular grid, each delta will have its unique semicircular grid size and consequently data frequency. Data binning of 10% of original data was later used as the basis of 'upstream-downstream' classification due to its proper representativity of the overall data without producing significant bias (see Supporting Information and Fig. S1 for details). The classifications of data into upstream and downstream parts were then used for bootstrap analysis of the dataset.

Bootstrapping distributary channel width distribution from modern river deltas

Bootstrapping was undertaken to assess the impact of a limited sample size, such as is often encountered when studying the rock record datasets due to exposure and, or, data availability. Bootstrapping is a resampling method that has been widely used in field studies with limited sample size (Cheng and Yeager, 2007; Cui et al., 2017; Debchoudhury et al., 2019). The method repeatedly resamples the original dataset with replacement (Efron, 1982; Efron, 2007). Resampling is repeated *B* times (*B* is typically a power of 10, e.g. 10, 100, 1000…) to transform a small number of measurements into a much larger sample size to improve the validity of statistical results obtained from analysing the data (Rice and Church, 1996; Cui et al., 2017).

In this study, rather than increasing the sample size from a large number of measured channel widths from modern river deltas, reverse bootstrapping was used to reduce the sample size to simulate the small number of distributary channel widths that can typically be measured from outcrops. Bootstrapping is used from 100% to 3% of the original number of distributary channel widths measured from modern deltas. Standard errors of these re-sampled datasets were then calculated show the distribution of standard errors for different sample sizes. Standard error (*S*) is defined as:

$$S = \frac{\sigma}{\sqrt{N}} \quad (1)$$

where σ is the standard deviation of channel widths (m) and *N* the number of measurements in the sample. *S*-*N* plots simulate the errors when measuring small numbers of distributary channel widths in the rock record. These relationships between sample size and standard error can be used both to inform sample size determination for field studies and also to quantify the uncertainties in measurements. Percentile standard errors were calculated to understand how the distribution of measured distributary channel widths influences the shape of the distribution of synthetic samples of different size. This analysis was designed to overcome the small sample sizes from ancient field

measurements through analysis of a large contemporary dataset; the influence of sample size on estimates of width is known for a normal distribution through equation (1), but using a large real dataset provides understanding of the influence of the shape of the underlying distribution on the results.

Delta width-discharge scaling

To provide new scaling relationships between channel width and total river discharge for river deltas, we use the same method as Prasojo et al. (2023) and relate the median channel widths of distributary channels for each delta to its bankfull discharge using log-log ordinary least squares (OLS) regression. This scaling does not allow calculation of the discharge/paleodischarge for a single distributary channel, but instead estimates the total riverine discharge that contributes to the building of the whole delta plain. We expand width-discharge scaling from river-dominated deltas from Prasojo et al. (2023) to also include wave- and tide-dominated deltas that and sub-divide each delta type based on downstream changes in dimensionless distributary channel width, as explained above. This approach provides more detailed width-discharge scaling relationships that consider marine influences on distal distributary channel widths.

All of the scaling relationships assume a power law relationship (i.e. linear on a log-log plot) between input river discharge and channel width (Leopold and Maddock, 1953). Median channel widths were used due to the width distributions being skewed, such that the median is more representative of the central tendency of the channel width population than the mean. Using the median channel width also reduces the influence of extreme values, so reducing the need to identify and exclude channels where tidal influence controls their width.

Median values of measured channel width (W_{med}) from each delta were plotted against the respective bankfull discharge values (Q_2). The discharge dataset was extracted from the Global Runoff Data Centre (GRDC), using the river gauges located closest to the delta apex. Bankfull

discharge is estimated from daily discharge data using Q_2, where 2 is the recurrence interval (years) of the discharge (see also Eaton, 2013; Jacobsen and Burr, 2016; Morgan and Craddock, 2019). Bankfull discharge is widely considered as the flow that controls channel geometry in alluvial rivers (de Rose et al., 2008; Haucke and Clancy, 2011; Gleason, 2015), although other factors (e.g. riverbank composition, grain size, slope) also affect this geometry. Calculations of Q_2 used the Flow Analysis Summary Statistics Tool (‘*fasstr’*) package for R (https://github.com/bcgov/fasstr). For some sites only monthly discharge data were available, from which daily equivalent Q_2 values were obtained using a climate-classified transformation (Supporting Information and Fig. S2; Beck et al., 2018).

Applying width-discharge scaling relationships to the rock record

To test the reliability of the scaling relationships produced in this study for application to the rock record, we utilized the ~400 km transect of the Cenomanian Mesa Rica Sandstone (Dakota Group, USA). The Mesa Rica Sandstone offers a rare example of an exhumed full-transect depositional profile of time-equivalent fluvio-deltaic strata, which is exposed in southeast Colorado and northeast New Mexico (Holbrook, 1996; Scott R.W. et al., 2004; Oboh-Ikuenobe et al., 2008; van Yperen et al., 2019; van Yperen et al., 2021). In east-central New Mexico, the Mesa Rica Sandstone (hereinafter referred to as ‘Mesa Rica’) is subdivided into lower, middle and upper units (Scott et al., 2004). The up-dip reaches of the lower Mesa Rica depositional system consist of single-story trunk channel deposits that form sheet like geometries with rare, abandoned channel-fill elements, which are interpreted to reflect deposition by single-thread channel streams (Holbrook, 1996; Holbrook, 2001). A down-dip transition from fluvial to deltaic deposits occurs at the northwestern rim of the Tucumcari sub-basin (Western Interior Basin). Here, the lower Mesa Rica consists of coalesced mouth-bar deposits overlain by amalgamated sandy distributary-channel deposits indicative of a river-dominated delta (van Yperen et al., 2019; Fig. 8 in van

Yperen et al., 2021). The interpretation of river-dominance is based on facies analyses and their respective depositional processes, thereby contrasting with morphology-based criteria used for modern deltas. During the Cretaceous, the study area was located at ~35°N latitude, with a warm and humid climate (Chumakov et al., 1995).

Distributary and trunk channel width measurements from the lower Mesa Rica (retrieved from van Yperen et al., 2019; 2021) consist of 13 data points distributed down-dip throughout the depositional system, from proximal (up-dip of the delta apex) to distal (Fig. 3; Table 2). Single channel deposits (both trunk and distributary) of the Mesa Rica are identified based on architectural analysis of channel elements and associated bounding surfaces from field sketches and photographs. These channel infill deposits are sand-prone and typically form amalgamated sandstone bodies (Holbrook, 2001; van Yperen et al., 2021). Only bounding scours that are continuous and strongly concave up on both sides of the enveloping channel fill elements are used for channel width measurements. Channel width measurements encompass the maximum distance between channel margins and provide apparent width measurements, as the outcrop exposure is at various angles to the true stream direction (van Yperen et al., 2019). Paleocurrent readings were grouped per study site, and average flow directions were used to reconstruct real channel widths trigonometrically (e.g. Fabuel-Perez et al., 2009; see Table S3 for details). Measured bankfull channel widths have an uncertainty factor of ± 4, arising from outcropping channel bodies cut at an angle to the reconstructed cross-stream direction (Hajek and Wolinsky, 2012; Blum et al., 2013; Holbrook and Wanas, 2014). The distributary channel widths were then plotted as dimensionless width (W^*) and dimensionless distance down-dip (s/L), assuming that the proximal channel width is represented by the width at the delta apex as the upstream limit of a delta plain. The reverse bootstrap method was then applied to this rock record dataset with a range of repetition numbers

(B = 1, 100, 1000, 10000). Subsequently, paleodischarges were estimated based on distributary channel widths using the empirical relationships generated in this study from modern deltas.

To test the reliability of these calculated paleodischarge estimates, we also estimated paleodischarge from trunk channels (n=4) using the flow velocity-based equation explained earlier. Paleohydrologic parameters for the Mesa Rica are used to estimate paleoslope (i.e. approximately 9.5×10^{-5} to 1.5×10^{-4}) and subsequent paleodischarge, assuming the value of 1.86 for bankfull dimensionless bed shear stress. The estimated paleoslope is then used to calculate the dimensionless Chézy friction coefficient, and therefore, paleodischarge (Parker, 1978; Parker, 2004). Formulae and details for the paleodischarge estimation using the flow velocity-based equation are provided in the Supporting Information (Table S1).

The flow velocity-based equation and the width-discharge scaling relationships developed in this study share the assumptions of the erosional geometry that defines the shape of the channel infill being in equilibrium with water discharge, and the paleochannel position being fixed. Preservation of a channel fill deposit requires aggradation, hence non-equilibrium conditions.

RESULTS

Down-dip changes in distributary channel widths

Description: Dimensionless widths from the distributary channels of 97 river-dominated deltas (Fig. 4A; Table S2, S4) show a gradual downstream decrease towards s/L = 0.1. A substantial increase in W^* with higher variance occurs at the shoreline, s/L = 0, in comparison to up-dip counterparts. The abrupt change in W^* distinguishes the upstream from the downstream part of the delta plain in these river-dominated deltas. The Kruskal-Wallis one-way analysis of variance test confirms this division between the upstream ($1 \leq s/L \leq 0.1$) and the downstream ($s/L = 0$) parts of river dominated deltas ($p < 0.05$).

Tide-dominated deltas (N = 7; Table S2, S4) show significant variability, but W^* increases towards the shoreline (Fig. 4B). There is a substantial increase of W^* at $s/L<0.5$ (Fig. 4B), that is taken as the transition between upstream and downstream parts of these deltas (Fig. 4E). In this case, the Kruskal-Wallis test corroborates this separation into upstream and downstream parts ($p < 0.05$).

The wave-dominated deltas (N = 10; Table S2, S4) show consistent dimensionless distributary channel widths across the upper parts ($s/L \geq 0.7$) of the delta plain (Fig. 4C), with an abrupt decrease at $s/L \sim 0.6$ (Fig. 4C) and a trend of increasing width further downstream. Nonetheless, there is no significant change in W^* between $1< s/L <0.7$ and $0.6< s/L <0$, so we do not sub-divide wave-dominated deltas into upstream and downstream regions. Due to the sample size being small with large variance, the Kruskal-Wallis test does not reject the null hypothesis ($p > 0.5$).

Interpretation: The abrupt and substantial increase of roughly double the median value of W^* at $s/L = 0$ in river-dominated deltas can be related to mouth-bar processes (Olariu and Bhattacharya, 2006). Mouth-bar deposition is mainly caused by a decrease in sediment carrying capacity due to the decreasing velocity of the river flow when it enters a standing body of seawater (Edmonds and Slingerland, 2007). Sediment carried by the distributary channels tends to be deposited along channel levees and also in a subaqueous mouth-bar that induces bifurcation as it grows (Fig. 4D, G; 'phase 2' of Olariu and Bhattacharya, 2006). As channels become shallower due to mouth bar growth, bank erosion accelerates so increasing the channel width at the river mouth, $s/L = 0$, as shown in this study. Fig. 4A shows that the median width of all upstream channels are around three times less than the median of all downstream channels located at $s/L = 0$, supporting the downstream widening pattern due to mouth bar growth hypothesis.

In tide-dominated deltas, there is a marked increase of W^* downstream of $s/L<0.5$ that results from the impact of tidal energy and associated backwater effects. The interaction between the unidirectional river flow and tidal currents within the standing body of seawater produces an interplay of physical (river, tides, waves), chemical (salinity), and biological (bioturbation) processes, seen in both modern and ancient systems (Dalrymple and Choi, 2007). To separate the upstream and downstream parts of tide-dominated deltas, we utilized the subzone classification of the fluvial-to-marine transition zone (FMTZ) (Gugliotta et al., 2016). The onset of the substantial increase of channel width downstream coincides with the boundary between the 'fluvially-dominated, tidally-influenced' and 'tidally-dominated, fluvially-influenced' zones of Gugliotta et al (2016). This boundary represents the sedimentological landward limit of tidal dominance. In the 'tidally-dominated, fluvially-influenced' zone, the role of river energy is predominantly to provide sediment. Additionally, the boundary position will shift landward and seaward due to the changes in the fluvial discharge (Dashtgard et al., 2012; Dalrymple et al., 2015; Jablonski and Dalrymple, 2016; Gugliotta et al., 2016) and cyclic fluctuations of tidal modulation (Allen et al., 1980; van den Berg et al., 2007; Dalrymple and Choi, 2007; Kravtsova et al., 2009). Even though each delta distributary channel could have a different FMTZ location, the boundary between the 'fluvially-dominated, tidally-influenced' and 'tidally-dominated, fluvially-influenced' zones is at $s/L = 0.45$ globally (Fig. 4B) where there is a statistically significant change in channel width.

Wave-dominated deltas occur in coastal settings with strong longshore currents that redistribute sediment away from the river mouth, producing different updrift and downdrift characteristics (Fig. 4F) (Bhattacharya and Giosan, 2003). Longshore wave energy tends to produce a single dominant distributary channel in these deltas (Korus and Fielding, 2015). Increasing the long-term wave energy relative to fluvial input will increase longshore sediment

dispersal, thereby reducing the rate of channel-belt aggradation and associated seaward extension and increasing the avulsion timescale by a factor of approximately 50 (Swenson, 2005). The increase in avulsion timescale, hence reduction in avulsion frequency, limits the growth of distributary networks as found in river- and tide-dominated deltas. Also, strong longshore wave energy tends to erode initial mouth bar deposits, hampering channel splitting due to mouth bar deposition. This absence of distal channel splitting explains the observed constant W^* from wave-dominated deltas from our global dataset (Fig. 4C). There is consequently no differentiation between upstream and downstream parts of wave-dominated deltas.

Bootstrapping estimation of sample standard error

Description: The standard error distributions for all delta types produced by bootstrapping dimensionless distributary channel widths show monotonic decreases with increasing number of measurements (Fig. 5A-E). The standard errors of dimensionless width (S_{w*}) estimates are significantly lower in the upstream parts of river-dominated deltas than in any of the other data sets (y-axis values in Fig. 5A-E). In contrast, the downstream parts of both river- and tide-dominated deltas consistently show the highest standard error values. These patterns reflect the data distributions (Fig. 4) and are also influenced by the number of measurements available in each case.

The implication of the low mean standard errors in the upstream parts of river-dominated deltas, where standard errors are consistently < 0.1 when $N > 30$ (using B=10; Fig. 5A), is that the standard error remains low (S_{w*}~0.2) with as few as three measurements (inset Fig. 5A). In the downstream parts of river-dominated deltas, the high variance of the 75 measured dimensionless channel widths leads to high standard errors (S_{w*} up to ~1) from 1000 bootstrap replications (B=1000) (Fig. 5B). The standard error reduces to 0.5 only when N is about 30 (inset Fig. 5B).

In tide-dominated deltas, upstream standard errors are lower (S_{w*}~0.4) than downstream (S_{w*}~2) from 1000 bootstrap replications (Fig. 5C, D). Only 6 data points are required to reduce the standard error (S_{w*}) to 0.5 (inset Fig. 5C). The standard errors in the downstream parts of tide-dominated deltas remain high for all sample sizes (i.e. S_{w*} = 1.5-3) (inset Fig. 5D).

In wave-dominated deltas the standard error reduces monotonically from 1000 bootstrap replications (Fig. 5E). Using five data points, S_{w*}~0.4 (inset Fig. 5E), and increasing the number of samples to 60 only reduces the standard error (S_{w*}) to 0.2.

The distributions of mean standard errors for each percentile are plotted in Fig. 5F-K. All the delta types consistently show asymmetry in standard errors for equivalent percentiles (P5-P95; P16-P84; P25-P75) around their respective P50 standard error distributions. Tide-dominated deltas show the largest difference between the percentiles, reflecting the skewed distribution of dimensionless distributary channel widths, while the upstream parts of river-dominated deltas reflect a lower skew in this distribution of dimensionless distributary channel widths.

Interpretation: In the upstream sections of river-dominated deltas where the unidirectional river current is dominant, changes in distributary channel patterns produced the lowest standard error in channel width compared to other delta types. At the other extreme, the lack of a dominant unidirectional river current, as in downstream parts of tide-dominated deltas, produces the highest standard errors (Fig. 5D) due to the higher variance in the measured distributary channel widths. Hence, as the data in Fig. 4 show, dimensionless channel widths are most consistent in river-dominated deltas, but marine influences, whether tidal or wave, lead to increased variability in widths and the standard error of width estimates increases as these non-fluvial factors become more dominant.

393 The positive skewness in dimensionless channel widths in all delta types and locations
394 (Fig. 4) has also been reported from fluvial outcrops and seismic sections (Colombera et al., 2019).
395 This suggests that statistical analyses of, and calculations using, channel widths measured from
396 river deltas or deltaic deposits should assume non-normal, positively skewed distributions.

397 ***Alternative delta hydraulic geometry models***

398 *Description:* Log-log plots (Fig. 6A-E) show power law relationships between the bankfull
399 discharge of the river upstream of the delta (Q_2) and median channel width for each delta (W_{med})
400 with Fig. 6F showing the power law relationship between the individual measured distributary
401 channels (W) and the bankfull discharge (Q_2). River- and wave- dominated deltas show how fluvial
402 hydraulic geometry theory (i.e. a significant, $p < 0.05$, positive power law relationship between
403 channel width and discharge) applies to these two delta types (Fig. 6A,B,E). However, in tide-
404 dominated deltas negative power law relationships are found (Fig. 6C,D), although these are not
405 statistically significant due to small sample sizes. Correlations are high in the upstream parts of
406 river-dominated, $Q_2 = 6.22W_{med}^{1.06}$ ($R^2 = 0.53$; s=0.46), and wave-dominated deltas, $Q_2 =$
407 $0.42W_{med}^{1.48}$ ($R^2 = 0.68$; s=0.43) (Fig. 6A, E). However, the downstream part of river-dominated
408 deltas has a lower R^2 (0.15; s=0.58) than the upstream counterparts (R^2=0.53). The residual
409 standard error of the regression (s) is higher in wave-dominated deltas due to smaller sample sizes.
410 Slope tests, comparing the regression slope to a specific value, were conducted to identify
411 the significance of differences between upstream and downstream regression lines of bankfull
412 discharge (Q_2) and median channel width (W_{med}) from river- and tide-dominated deltas. We also
413 compared the regression lines from each delta type to the global W-Q_2 equation shown in Fig. 6F.
414 The slope tests are significant ($p < 0.05$) for all of these comparisons, such that: (a) the slopes of
415 the median width – Q relationships for river- and wave-dominated deltas are significantly steeper

than for the global data set of individual measurements; and, (b) the Q_2-W_{med} relationship is steeper for the upstream parts of river dominated deltas than that for the downstream parts. The large sample size means that the 95% confidence interval in Fig. 6F is narrow (±81.37 m^3/s), showing the statistical strength of the distributary channel width to bankfull discharge scaling across three orders of magnitude of discharge values.

Interpretation: The scatter in median width-discharge data (Fig. 6) increases (and, although affected by sample size, so does the regression standard error, *s*) where marine energy (tides, longshore currents, waves) is greater, and that this energy directly impacts distributary channel width. Tidal energy obstructs the down-delta flow and causes distal widening, reflected in the distribution of distributary channel widths (Fig. 4B) and the standard errors of width estimates derived from samples (Fig. 5C,D).

Mouth-bar deposition also affects channel width in the downstream part of river-dominated deltas (Fig. 4A, 5B, 6B), as noted by Olariu and Bhattacharya (2006). Subaqueous mouth-bar deposition triggers a drop in transport capacity due to jet expansion and flow deceleration, hence producing relatively wider distributary channels than in the upstream part. Upstream of any influence of marine energy, channel width is directly related to the scale of the supplying river system (Fig. 4A,C, 5A,E, 6A,E). Longshore wave energy and sediment redistribution do not significantly affect the distributary channel width in wave-dominated deltas (Fig. 4C), thus river discharge retains a significant influence and a statistically significant width-discharge scaling relationship is found (Fig. 6E). Fig. 6E shows how the 95% confidence interval is narrow (±81.37 m^3/s) which is comparable with Prasojo et al. (2023) (±52 m3/s),even though more width measurements were added in this study. Power law relationships between W_{med} and Q_2 produced here can be used to calculate the total riverine discharge that contributes sediment to building the

delta plain, but do not allow prediction of the discharge/paleodischarge value of a single distributary channel. These results imply that the principles of hydraulic geometry scaling are applicable to river- and wave-dominated deltas but not to tide-dominated deltas. However, our tide-dominated deltas dataset is small (N = 7), hence adding more data may change this interpretation. Moreover, since the slope tests show significant differences between upstream-downstream, and also between each delta type and the global W-Q_2 scaling, the individual scaling relationships (Fig. 6) cannot be used interchangeably.

Testing alternative width-discharge scaling relationships on a rock record case study

Description: In total, 13 distributary channels were measured at locations across a delta identified in the lower Mesa Rica (Fig. 7A; Table 2). Down-dip decreasing distributary channel widths are observed even though this decrease is not statistically significant (Wilcoxon test $p > 0.05$, variance test $p > 0.05$). The whole sample shows a bimodal distribution of widths (Fig. 7B). As the proximal zone contains only one measurement, which is from a trunk channel, we can neglect this zone because it is not part of the distributive system on the delta plain. Consequently, we use the distributary channel widths measured from the transitional (N=5) and the distal zones (N=7) which show skewed distributions (Fig. 7B). Applying the bootstrap method to the dimensionless distributary channel widths measured from the transitional and distal parts produced low standard error (S_{w*} ~0.13-0.18) from 1000 bootstrap replicates (B) (Fig. 7C). The standard error remains low (~0.18) when using only the seven measurements from the lower Mesa Rica (Fig. 7C).

Interpretation: The delta front sandstone bodies of the lower Mesa Rica are interpreted as the product of deposition dominated by river influence (van Yperen et al., 2019). Down-dip decreasing distributary channel widths are similar to downstream trends in channel width from

proximal parts of modern river-dominated deltas (Fig. 4A). To calculate paleodischarge from the distributary channels of the lower Mesa Rica, the median channel width of 12 measured distributary channel widths, 109 m, was put into the hydraulic geometry equation obtained above for the proximal part (in the rock record terms) or upstream part (in modern system terms) of river-dominated deltas, $Q_2 = 6.22W_{med}^{1.06}$ (Fig. 6A) giving $Q_2 = 898 \pm 4741$ m^3/s (i.e. ± showing 95% prediction interval from the regression line shown in Fig. 6A). The flow velocity-based method, applied on trunk channel deposits (n=4), produces a range of $Q_2 = 1085$-1392 m^3/s (with central estimate of 1244 m^3/s; see Table S1 and Supporting Information for details). These estimates from two different methods overlap (i.e. the hydraulic geometry equation, this study, and the flow velocity-method (Holbrook and Wanas, 2014; Bhattacharya et al., 2016), although the central estimate that we obtained is ~10% lower than obtained from the flow velocity-based method.

DISCUSSION

Down-dip changes in distributary channel width in modern and ancient deltas

Modern deltas perspective. From 6213 measured channel widths across globally distributed deltas of different types in various climate regions, it is shown that marine processes (waves, tides, longshore currents) influence the distributary channel widths differently according to the type of delta. In river-dominated deltas, the data consistently show that channel width decreases down-dip before a sharp increase at the shoreline due to mouth-bar deposition (Fig. 4A). Olariu and Bhattacharya (2006) also found a similar pattern of distributary channel widths in the Trovimovskaya River, a distributary channel from the river-dominated Lena delta. In tide-dominated deltas, tides lead to increased channel widths up to around half of the distance from the shoreline to the delta apex, consistent with observations made for several geometrical properties (channel curvature, width/depth ratio, bed level, bifurcation order) in the Kapuas, Mahakam and Mekong modern deltas (Sassi et al., 2012; Kästner et al., 2017; Gugliotta et al., 2019). Longshore

currents in wave-dominated deltas lead to lateral sediment redistribution parallel to the shoreline and formation of a cuspate geometry, rather than in the down-dip direction. However, these marine processes do not produce statistically significant down-dip changes of channel widths in wave-dominated deltas. Understanding the boundaries between upstream and downstream sections across different delta types is a requirement to apply the hydraulic geometry models we proposed from modern systems. Even with further information from bedforms and fossils, finding the upstream-downstream patterns from deep time delta deposits remain challenging, considering the fact that hydraulic geometry produces significantly different scaling ($p < 0.05$) in each delta type.

Ancient delta perspective.---This study has demonstrated both the overall controls over channel width and down-dip patterns of distributary channel widths from modern systems and how this information can be used in interpreting ancient systems. Limited exposure often prevents the collection of large numbers of channel width measurements from ancient fluvio-deltaic strata. The 6213 measurements from modern distributary channels allow us to simulate the consequences of sampling limited numbers of distributary channel widths in the rock record. Using bootstrapping, we simulate standard error distributions that may be expected when limited numbers of channel widths are able to be measured from outcrops. If it is possible to identify the relative down-delta position of measurements, specific width-discharge relationships are available and the uncertainties in estimating discharge can be determined. As well as quantifying uncertainty, these results can be used in field work planning by enabling dynamic estimation of the number of samples required as data are gathered.

The lower Mesa Rica provides an example of how the down-dip pattern of distributary channel widths could be retrieved from the rock record and compared with modern systems. By having the down-dip pattern along with the context of the depositional setting determined from

sedimentary structures and facies distributions, the same bootstrapping method to reduce the number of samples could produce a range of standard error values that could be expected from a rock record case study (Fig. 7C). The equation developed for the upstream parts of river-dominated deltas was then used to estimate the paleodischarge from this formation due to abundant evidence of river domination. In the absence of evidence concerning the delta type or location of the measurements, paleodischarge calculations can be made using Prasojo et al. (2023) models.

Standard error distribution of deltas distributary channel widths.---Fig. 5 shows the relationships between the number of measured distributary channel widths and the mean standard error using a bootstrapping method. In river- and wave-dominated deltas, low standard errors of dimensionless width occur (Fig. 5A,B,E). These low errors imply that reliable estimates of median channel width can be obtained from a small number of measurements, with the aims of the study determining the acceptable uncertainty for a given number of measurements. However, for tide-dominated deltas it is challenging to produce reliable width estimates that can be related to input river discharge due to the significant influence of tidal energy on channel form. Even with 30 data points in the downstream part of tide-dominated deltas, the standard error of dimensionless width remains high (S_w*>1). Thus, caution should be taken when applying tide-dominated delta discharge-width scaling relationship from either the modern system or even with a thorough facies analyses from the rock record.

Channel width distributions across all delta types are positively skewed, implying that mean distributary channel width may not be statistically representative (Fig. 5G-K) and that median values are better representative values of channel width. This has implications for the application of other scaling relationships where small sample sizes are available; many such relationships are used including those with catchment area, meander wavelength, channel

sinuosity, total river-atmosphere carbon dioxide flux, mean and peak discharge, and sediment transport mode (Leopold and Maddock, 1953; Bridge and Mackey, 1993; Bhatt and Tiwari, 2008; Gleason et al., 2018; Allen and Pavelsky, 2018; Frasson et al., 2019; Dunne and Jerolmack, 2020; Lyster et al., 2021).

Comparing width-discharge relationships with the flow velocity-based equations.---Bankfull paleodischarge estimated using the width-discharge relationship from distributary channels on modern delta plains in this study lie within ~10% of those obtained from Mesa Rica trunk channel deposits using the flow velocity-based equations. Their uncertainty ranges overlap significantly, suggesting that these approaches are consistent, although they were calculated based on different channels (i.e. our new scaling is applied to distributary channels and flow velocity-based equations were applied to trunk channels). Our estimated paleodischarge using width-discharge relationship is less than the paleodischarge estimated using the flow velocity-based equations by around 10% because of the decrease of slope, the encounter with slope break and/or the backwater effect will reduce the total estimated discharge in distributary channels compared to the trunk channel (Paola and Mohrig, 1996; Ganti et al., 2016; Prasojo et al., 2022).

The distributary channel deposits that our new scaling relationships are based on are interpreted to represent deposition on the proximal delta plain (Van Yperen et al., 2019). This contrasts with the trunk channel deposits which are utilized for the flow velocity-based equations and are interpreted to reflect deposition in the proximal reaches of the backwater zone (Van Yperen et al., 2021). Their laterally continuous sheet-forming architecture is the product of entering the backwater zone, as this increases avulsion and limits channel incision and/or aggradation (van Yperen et al., 2021). The proximal reaches of the backwater zone (i.e. trunk channel deposition) and the proximal delta plain (i.e. distributary channel deposition) reflect similar environments

555 where the effect of backwater effect and mouth-bar deposition have not taken an effect in this part
556 of river-dominated delta. Hence, the results from the independent methods are comparable.

557 Our method uses only a single parameter, channel width, whereas the flow velocity-based
558 equations use estimates of bankfull channel depth and width, paleoslope, mean bedform height
559 and wavelength (Bridge and Tye, 2000; Leclair and Bridge, 2001; Holbrook and Wanas, 2014;
560 Trampush et al., 2014). As well as relying on a single input parameter, where stratigraphic data
561 are available, our method allows estimates to be tailored to delta type and the along-dip location
562 of the measured widths.

563 Further data will allow systematic down-dip scaling relationships to potentially be
564 developed for other channel types, such as tidal creeks, and may enable further differentiation of
565 delta types. Similar work has been undertaken in modern estuaries (Diefenderfer et al., 2008; Gisen
566 and Savenije, 2015) and tide-influenced deltas (Sassi et al., 2012). Improved understanding at the
567 system scale is important to further source-to-sink analyses and hence improve volumetric
568 assessment of resource reservoirs, and carbon capture and storage facilities, as well as deducing
569 climate and tectonic forcing and refining paleohydraulic reconstructions (Montgomery and Gran,
570 2001; Merritt and Wohl, 2003; Bhattacharya and Tye, 2004; Brardinoni and Hassan, 2006; Wohl
571 and David, 2008; Davidson and Hartley, 2010; Eaton, 2013).

572 **Limitations of applying modern delta scaling relationships to the rock record**.---We show that
573 distributary channel width (W_{med}) from modern deltas scales with input river bankfull discharge
574 (Q_2) from our global dataset (Fig. 6F). However, this study provides empirical evidence of how
575 deltaic width-discharge scaling relationships start to weaken with the increasing influence of
576 marine processes that directly influence hydraulic and sediment processes (Fig. 6A-E). Scaling
577 relationships derived from the upstream parts of modern river-dominated deltas, from which

578 marine influence is largely absent, show strong statistical correlation between median channel
579 width and input river discharge ($R^2 = 0.53$; $p < 0.05$) (Fig. 6A). The correlations are weaker ($R^2 =$
580 0.15; $p < 0.05$) for downstream parts of river dominated deltas and stronger ($R^2 = 0.68$; $p < 0.05$)
581 for wave-dominated deltas and becomes statistically insignificant in the upstream part of tide-
582 dominated deltas ($R^2 = 0.03$; $p > 0.05$), and downstream tide-dominated deltas ($R^2 = 0.01$; $p > 0.05$)
583 (Fig. 6A-E). The trend for correlation to decrease with increased marine influence (e.g. tidal, wave
584 or backwater-controlled flow regimes) is anticipated, and existing hydraulic geometry models
585 assume unidirectional river flow (Gleason and Smith, 2014). However, in wave–dominated
586 systems the wave energy appears to have minimal impact on channel widths, and thus significant
587 width-discharge scaling relationships can still be obtained (Fig. 6E).

588 Reconstructing water discharge of an ancient fluvial and/or delta system relies on accurate
589 measurement of channel geometry from channel fills (Parker et al., 2007; Hayden et al., 2019). In
590 outcrop or subsurface datasets, it is commonly easier to measure distributary channel depths than
591 widths. However, whereas very accurate width measurements can be made from satellite images
592 as in this study, depth requires to be estimated from water color on the images which is difficult to
593 calibrate and subject to significant errors especially in deeper water bodies (Geyman and Maloof,
594 2019). An alternative approach is to obtain width-depth empirical relationships from field
595 measurements in modern river deltas and use these to transform width-discharge to depth-
596 discharge relationships. On the other hand, several issues influence the accuracy of width
597 measurements from outcrops. The measured channel fill may not be perpendicular to the paleoflow
598 (Holbrook and Wanas, 2014; Bhattacharya et al., 2016) and infill deposits are often incompletely
599 preserved (Bridge and Mackey, 1993; Bridge and Tye, 2000). When the channel fill deposit is
600 incomplete, width-depth scaling relationships can still be used, albeit with increased uncertainty

601 because channel fill dimensions can differ significantly from formative channel dimensions
602 (Hayden et al., 2019; Greenberg et al., 2021).

603 The proposed scaling relationships should not be used as a standalone model to interpret
604 paleodischarge from the rock record. Uncertainties exist in both the field data and the statistical
605 relationships; hence, the results provide discharge ranges based on the propagation of these
606 uncertainties. Additional information should be gathered from outcrops to further constrain the
607 predicted paleodischarge; this may include stratigraphic context, sedimentary structures, grain
608 size, fossil assemblages and vegetation, amongst others. As an example, using the scaling
609 relationship for the upstream part of river-dominated deltas (Fig. 6A), a median distributary
610 channel width of 300 m gives a discharge range of $Q_2 = 2627 \pm 17942$ m^3/s (i.e. ± is from the 95%
611 prediction interval produced by regression line on Fig. 6A; note that this interval increases away
612 from the mean of the data). The uncertainty in paleodischarge values is considerably greater in
613 marine-influenced deltas, namely the downstream part of river-dominated deltas or wave-
614 dominated deltas. Thus, the interpretation of paleodischarge requires contextual information that
615 may support or challenge the calculated values.

616 In order to assess paleodischarge estimates using our approach, we utilize the case study
617 from the lower Mesa Rica. The coastal plain of the lower Mesa Rica delta is approximately 100
618 km long, based on the approximated shoreline position at maximum regression (i.e. oceanward
619 migration of the shoreline) and the most proximal occurrence of distributary channel deposits (Fig.
620 3). In terms of delta plain size, the lower Mesa Rica is comparable with the modern Brahmani
621 (1800 km^2) and Mahanadi (1700 km^2) deltas, although in terms of average bankfull channel depth
622 (Table S1), the smaller Danube (5800 km^2), Ebro (460 km^2) and Mahanadi are better comparisons.
623 The discharge of the lower Mesa Rica is more comparable to total system discharge coming into

Ebro, Cauvery, Wax Lake, Sanaga and Rio Sinú deltas (GRDC; Bhattacharya and Tye, 2004). These comparisons indicate that the lower Mesa Rica is comparable with many modern deltas but none of them provides a perfect fit in terms of geometry (delta area, bankfull channel depth) and input discharge. The number and diversity of potential modern delta analogues for the Mesa Rica illustrates how scaling relationships from modern systems should not be used in isolation.

The difference in widths in river-dominated deltas between their upstream and downstream parts leads to differences in the statistical significance and uncertainty associated with scaling relationships for the two parts. Consequently, the number of measurements required to estimate input discharge to a specified level of uncertainty varies with the location of measurements along the delta. In some well-studied systems this specification of location is possible, potentially alongside information on climate type, and thus the methods shown in this study are applicable. Where context is unknown the scaling relationships provided here should be used with caution.

CONCLUSION

Distinct down-dip patterns of dimensionless distributary channel widths are recognized from measurements from 114 modern global river deltas. River- and tide-dominated deltas show significant channel widening at $s/L = 0.05$ (i.e. near shoreline) and 0.45 (i.e. approximately halfway across the delta plain from the shoreline to the apex), respectively. Mouth bar depositional cycles in river-dominated deltas and tidal energy obstructing unidirectionality of channel currents in tide-dominated deltas are the main cause of these distinct patterns. In contrast, wave-dominated deltas show consistent dimensionless distributary channel width down-dip. Calculation of paleodischarge based on empirical relationships between median channel width and input river discharge produce statistically significant width-discharge scaling relationships for upstream river- and wave-dominated deltas, with no significant relationships identified for downstream river- and tide-

dominated deltas. By bootstrapping the dimensionless distributary channel widths from modern deltas, this study provides estimates of the minimum number of measurements required to estimate median width to a specified standard error. We calculate the minimum number of measurements (N_{min}) required to reduce the standard error of dimensionless width to 0.5 as follows: upstream (N_{min} = 3) and downstream (N_{min} = 30) of river-dominated deltas; upstream part of tide-dominated deltas (N_{min} = 6); and, wave-dominated deltas (N_{min} = 4). The downstream part of tide-dominated deltas produces very high standard error (>1.5) with any number of samples and input discharge cannot be reliably estimated from channels in these locations. Applying the proposed distributary channel width-discharge scaling relationships from modern deltas to the lower Mesa Rica produced a comparable paleodischarge estimate to that from the flow velocity-based method. The results from this study can be used to improve paleoclimate and tectonic reconstruction, volumetric assessment of hydrocarbon, hydrogen and geothermal reservoirs, in diverse depositional environments. The results also enable more detailed paleohydraulic reconstruction across various types of depositional systems in source-to-sink investigations.

ACKNOWLEDGMENTS

We thank Ivar Midtkandal (University of Oslo) who initiated collaboration between Anna van Yperen and the University of Glasgow. The research was funded by The Indonesia Endowment Fund for Education (LPDP) awarded to Prasojo. Authors also thank editor, Prof. Kathleen M. Marsaglia, associate editor, Dr Douglas Edmonds, and reviewer Dr Sinéad Lyster and other anonymous reviewers who have made significant contributions to the quality of the manuscript.

DATA AVAILABILITY STATEMENT

Data from this paper (Table S2) are available in the open repository (https://doi.org/10.6084/m9.figshare.19964549.v4). Information about date of Landsat5 used in this study is available in the open repository (https://doi.org/10.6084/m9.figshare.24119622.v1). The global river discharge data set is available from The Global Runoff Data Centre (GRDC), 56068 Koblenz, Germany via the web (https://www.bafg.de/GRDC/EN/02_srvcs/21_tmsrs/210_prtl/prtl_node.html).

REFERENCES

Allen, G.H., and Pavelsky, T.M., 2018, Global extent of rivers and streams: Science, v. 361, no. 6402, p. 585–588.

Allen, G.P., Salomon, J.C., Bassoullet, P., du Penhoat, Y., and de Grandpré, C., 1980, Effects of tides on mixing and suspended sediment transport in macrotidal estuaries: Sedimentary Geology, v. 26, nos. 1–3, p. 69–90.

Allen, P.A., Armitage, J.J., Carter, A., Duller, R.A., Michael, N.A., Sinclair, H.D., Whitchurch, A.L., and Whittaker, A.C., 2013, The Qs problem: Sediment volumetric balance of proximal foreland basin systems: Sedimentology, v. 60, no. 1, p. 102–130.

Beck, H.E., Zimmermann, N.E., McVicar, T.R., Vergopolan, N., Berg, A., and Wood, E.F., 2018, Present and future köppen-geiger climate classification maps at 1-km resolution: Scientific Data, v. 5, no. 1, p. 1–12.

van den Berg, J.H., Boersma, J.R., and van Gelder, A., 2007, Diagnostic sedimentary structures of the fluvial-tidal transition zone - Evidence from deposits of the Rhine and Meuse: Geologie en Mijnbouw/Netherlands Journal of Geosciences, v. 86, no. 3, p. 287–306.

690 Besset, M., Anthony, E.J., and Sabatier, F., 2017, River delta shoreline reworking and erosion in
691 the Mediterranean and Black Seas: the potential roles of fluvial sediment starvation and other
692 factors: Elem Sci Anth, v. 5, no. 0, p. 54.
693 Bhatt, V.K., and Tiwari, A.K., 2008, Estimation of peak streamflows through channel geometry /
694 Estimation de pics de débit fluviatiles à l'aide de la géométrie des cours d'eau Estimation of
695 peak streamflows through channel geometry: Hydrological Sciences-Journal-des Sciences
696 Hydrologiques, v. 53, no. 2, p. 401–408.
697 Bhattacharya, J.P., 2006, Deltas: SEPM (Society for Sedimentary Geology), 237–292 p.
698 Bhattacharya, J.P., and Giosan, L., 2003, Wave-influenced deltas: Geomorphological implications
699 for facies reconstruction: Sedimentology, v. 50, no. 1, p. 187–210.
700 Bhattacharya, J.P., and Tye, R.S., 2004, Searching for modern Ferron analogs and application to
701 subsurface interpretation, in Chidsey, T.C., Adams, R.D., and Morris, T.H. eds., Regional to
702 Wellbore Analog for Fluvial–Deltaic Reservoir Modeling: the Ferron Sandstone of Utah:
703 American Association of Petroleum Geologists, Studies in Geology 50: American
704 Association of Petroleum Geologists, p. 39–57.
705 Bhattacharya, J.P., Copeland, P., Lawton, T.F., and Holbrook, J., 2016, Estimation of source area,
706 river paleo-discharge, paleoslope, and sediment budgets of linked deep-time depositional
707 systems and implications for hydrocarbon potential: Earth-Science Reviews, v. 153, p. 77–
708 110.
709 Blum, M., Martin, J., Milliken, K., and Garvin, M., 2013, Paleovalley systems: Insights from
710 Quaternary analogs and experiments: Earth-Science Reviews, v. 116, no. 1, p. 128–169.
711 Blum, M.D., and Törnqvist, T., 2000, Fluvial responses to climate and sea-level change: a review
712 and look forward: Sedimentology, v. 47, no. s1, p. 2–48.

713 Brardinoni, F., and Hassan, M.A., 2006, Glacial erosion, evolution of river long profiles, and the
714 organization of process domains in mountain drainage basins of coastal British Columbia:
715 Journal of Geophysical Research, v. 111, no. F1, p. F01013.
716 Brewer, C.J., Hampson, G.J., Whittaker, A.C., Roberts, G.G., and Watkins, S.E., 2020,
717 Comparison of methods to estimate sediment flux in ancient sediment routing systems: Earth-
718 Science Reviews, v. 207, p. 103217.
719 Bridge, J.S., and Mackey, S.D., 1993, A theoretical study of fluvial sandstone body dimensions,
720 in The Geological Modelling of Hydrocarbon Reservoirs and Outcrop Analogues: wiley, p.
721 213–236.
722 Bridge, J.S., and Tye, R.S., 2000, Interpreting the Dimensions of Ancient Fluvial Channel Bars,
723 Channels, and Channel Belts from Wireline-Logs and Cores: AAPG Bulletin, v. 84, no. 8, p.
724 1205–1228.
725 Caldwell, R.L., Edmonds, D.A., Baumgardner, S., Paola, C., Roy, S., and Nienhuis, J.H., 2019, A
726 global delta dataset and the environmental variables that predict delta formation on marine
727 coastlines: Earth Surface Dynamics, v. 7, no. 3, p. 773–787.
728 Castelltort, S., Goren, L., Willett, S.D., Champagnac, J.D., Herman, F., and Braun, J., 2012, River
729 drainage patterns in the New Zealand Alps primarily controlled by plate tectonic strain:
730 Nature Geoscience, v. 5, no. 10, p. 744–748.
731 Chadwick, A.J., Lamb, M.P., Moodie, A.J., Parker, G., and Nittrouer, J.A., 2019, Origin of a
732 Preferential Avulsion Node on Lowland River Deltas: Geophysical Research Letters, v. 46,
733 no. 8, p. 4267–4277.

Chadwick, A.J., Lamb, M.P., and Ganti, V., 2020, Accelerated river avulsion frequency on lowland deltas due to sea-level rise: Proceedings of the National Academy of Sciences of the United States of America, v. 117, no. 30, p. 17584–17590.

Chatanantavet, P., Lamb, M.P., and Nittrouer, J.A., 2012, Backwater controls of avulsion location on deltas: Geophysical Research Letters, v. 39, no. 1, p. 2–7.

Cheng, A., and Yeager, M., 2007, Bootstrap resampling for voxel-wise variance analysis of three-dimensional density maps derived by image analysis of two-dimensional crystals: Journal of Structural Biology, v. 158, no. 1, p. 19–32.

Chumakov, N., Zharkov, M.A., Herman, A.B., Doludenko, M.P., Kalandadze, N.N., Lebedev, E.L., Ponomarenko, A.G., and Rautian, A.S., 1995, Climatic Belts of the Mid-Cretaceous Time: Stratigraphy and Geological Correlation, v. 3, no. 3, p. 42–63.

Colombera, L., Mountney, N.P., Medici, G., and West, L.J., 2019, The geometry of fluvial channel bodies: Empirical characterization and implications for object-based models of the subsurface: AAPG Bulletin, v. 103, no. 4, p. 905–929.

Cui, M., Xu, L., Wang, H., Ju, S., Xu, S., and Jing, R., 2017, Combining Nordtest method and bootstrap resampling for measurement uncertainty estimation of hematology analytes in a medical laboratory: Clinical Biochemistry, v. 50, no. 18, p. 1067–1072.

Dalrymple, R.W., and Choi, K., 2007, Morphologic and facies trends through the fluvial-marine transition in tide-dominated depositional systems: A schematic framework for environmental and sequence-stratigraphic interpretation: Earth-Science Reviews, v. 81, nos. 3–4, p. 135–174.

755 Dalrymple, R.W., Kurcinka, C.E., Jablonski, B.V.J., Ichaso, A.A., and Mackay, D.A., 2015,
756 Deciphering the relative importance of fluvial and tidal processes in the fluvial-marine
757 transition, in Developments in Sedimentology: Elsevier, p. 3–45.
758 Dashtgard, S.E., Venditti, J.G., Hill, P.R., Sisulak, C.F., Johnson, S.M., and Croix, A.D. la, 2012,
759 Sedimentation Across the Tidal-Fluvial Transition in the Lower Fraser River, Canada: The
760 Sedimentary Record.
761 Davidson, S.K., and Hartley, A.J., 2010, Towards a quantitative method for estimating
762 paleohydrology from clast size and comparison with modern rivers: Journal of Sedimentary
763 Research, v. 80, nos. 7–8, p. 688–702.
764 Davidson, S.K., and North, C.P., 2009, Geomorphological regional curves for prediction of
765 drainage area and screening modern analogues for rivers in the rock record: Journal of
766 Sedimentary Research, v. 79, no. 10, p. 773–792.
767 Debchoudhury, S., Sengupta, S., Earle, G., and Coley, W., 2019, A Bootstrap-Based Approach for
768 Improving Measurements by Retarding Potential Analyzers: Journal of Geophysical
769 Research: Space Physics, v. 124, no. 6, p. 4569–4584.
770 Diefenderfer, H.L., Coleman, A.M., Borde, A.B., and Sinks, I.A., 2008, Hydraulic geometry and
771 microtopography of tidal freshwater forested wetlands and implications for restoration,
772 Columbia River, U.S.A.: Ecohydrology and Hydrobiology, v. 8, nos. 2–4, p. 339–361.
773 Duller, R.A., Whittaker, A.C., Fedele, J.J., Whitchurch, A.L., Springett, J., Smithells, R., Fordyce,
774 S., and Allen, P.A., 2010, From grain size to tectonics: Journal of Geophysical Research:
775 Earth Surface, v. 115, no. 3, p. 3022.
776 Dunne, K.B.J., and Jerolmack, D.J., 2020, What sets river width? Science Advances, v. 6, no. 41,
777 p. eabc1505.

778 Eaton, B.C., 2013, Hydraulic Geometry: Empirical Investigations and Theoretical Approaches, in
779 Treatise on Geomorphology: Elsevier Inc., p. 313–329.
780 Edmonds, D.A., and Slingerland, R.L., 2007, Mechanics of river mouth bar formation:
781 Implications for the morphodynamics of delta distributary networks: Journal of Geophysical
782 Research: Earth Surface, v. 112, no. 2.
783 Efron, B., 1982, The Jackknife, the Bootstrap and Other Resampling Plans: Society for Industrial
784 and Applied Mathematics.
785 Efron, B., 2007, Bootstrap Methods: Another Look at the Jackknife: The Annals of Statistics, v.
786 7, no. 1, p. 1–26.
787 Eide, C.H., Müller, R., and Helland-Hansen, W., 2018, Using climate to relate water discharge and
788 area in modern and ancient catchments (V. Manville, Ed.): Sedimentology, v. 65, no. 4, p.
789 1378–1389.
790 Fabuel-Perez, I., Hodgetts, D., and Redfern, J., 2009, A new approach for outcrop characterization
791 and geostatistical analysis of a low-sinuosity fluvial-dominated succession using digital
792 outcrop models: Upper Triassic Oukaimeden Sandstone Formation, central High Atlas,
793 Morocco: AAPG Bulletin, v. 93, no. 6, p. 795–827.
794 Fernandes, A.M., Törnqvist, T.E., Straub, K.M., and Mohrig, D., 2016, Connecting the backwater
795 hydraulics of coastal rivers to fluviodeltaic sedimentology and stratigraphy: Geology, v. 44,
796 no. 12, p. 979–982.
797 Finzel, E.S., 2014, Detrital zircons from Cretaceous midcontinent strata reveal an Appalachian
798 Mountains–Cordilleran foreland basin connection: Lithosphere, v. 6, no. 5, p. 378–382.
799 Frasson, R.P. de M., Pavelsky, T.M., Fonstad, M.A., Durand, M.T., Allen, G.H., Schumann, G.,
800 Lion, C., Beighley, R.E., and Yang, X., 2019, Global Relationships Between River Width,

Slope, Catchment Area, Meander Wavelength, Sinuosity, and Discharge: Geophysical Research Letters, v. 46, no. 6, p. 3252–3262.

Galloway, W.D., 1975, Process Framework for describing the morphologic and stratigraphic evolution of deltaic depositional systems: Houston Geological Society. Deltas: Models for Exploration, no. September, p. 87–98.

Ganti, V., Chadwick, A.J., Hassenruck-Gudipati, H.J., Fuller, B.M., and Lamb, M.P., 2016, Experimental river delta size set by multiple floods and backwater hydrodynamics: Science Advances, v. 2, no. 5, p. e1501768.

Geyman, E.C., and Maloof, A.C., 2019, A Simple Method for Extracting Water Depth From Multispectral Satellite Imagery in Regions of Variable Bottom Type: Earth and Space Science, v. 6, no. 3, p. 527–537.

Gisen, J.I.A., and Savenije, H.H.G., 2015, Estimating bankfull discharge and depth in ungauged estuaries: Water Resources Research, v. 51, no. 4, p. 2298–2316.

Gleason, C.J., 2015, Hydraulic geometry of natural rivers: A review and future directions: Progress in Physical Geography, v. 39, no. 3, p. 337–360.

Gleason, C.J., Wada, Y., and Wang, J., 2018, A Hybrid of Optical Remote Sensing and Hydrological Modeling Improves Water Balance Estimation: Journal of Advances in Modeling Earth Systems, v. 10, no. 1, p. 2–17.

Greenberg, E., Ganti, V., and Hajek, E., 2021, Quantifying bankfull flow width using preserved bar clinoforms from fluvial strata: Geology, v. 1.

Gugliotta, M., and Saito, Y., 2019, Matching trends in channel width, sinuosity, and depth along the fluvial to marine transition zone of tide-dominated river deltas: The need for a revision of depositional and hydraulic models: Earth-Science Reviews, v. 191, no. January, p. 93–113.

824 Gugliotta, M., Flint, S.S., Hodgson, D.M., and Veiga, G.D., 2016, Recognition criteria,
825 characteristics and implications of the fluvial to marine transition zone in ancient deltaic
826 deposits (Lajas Formation, Argentina): Sedimentology, v. 63, no. 7, p. 1971–2001.
827 Gugliotta, M., Saito, Y., Nguyen, V.L., Ta, T.K.O., and Tamura, T., 2019, Sediment distribution
828 and depositional processes along the fluvial to marine transition zone of the Mekong River
829 delta, Vietnam: Sedimentology, v. 66, no. 1, p. 146–164.
830 Hack, J.T., 1973, Stream-profile analysis and stream-gradient index: Journal of Research of the
831 U.S. Geological Survey, v. 1, no. 4, p. 421–429.
832 Hajek, E.A., and Wolinsky, M.A., 2012, Simplified process modeling of river avulsion and alluvial
833 architecture: Connecting models and field data: Sedimentary Geology, v. 257–260, p. 1–30.
834 Hampson, G.J., Jewell, T.O., Irfan, N., Gani, M.R., and Bracken, B., 2013, Modest change in
835 fluvial style with varying accommodation in regressive alluvial-to-coastal-plain wedge:
836 Upper Cretaceous Blackhawk Formation, Wasatch Plateau, central Utah, U.S.A: Journal of
837 Sedimentary Research, v. 83, no. 2, p. 145–169.
838 Hartley, A.J., Weissmann, G.S., and Scuderi, L., 2017, Controls on the apex location of large
839 deltas: Journal of the Geological Society, v. 174, no. 1, p. 10–13.
840 Haucke, J., and Clancy, K.A., 2011, Stationarity of streamflow records and their influence on
841 bankfull regional curves: Journal of the American Water Resources Association, v. 47, no. 6,
842 p. 1338–1347.
843 Hayden, A.T., Lamb, M.P., Fischer, W.W., Ewing, R.C., McElroy, B.J., and Williams, R.M.E.,
844 2019, Formation of sinuous ridges by inversion of river-channel belts in Utah, USA, with
845 implications for Mars: Icarus, v. 332, p. 92–110.

846 Holbrook, J., 2001, Origin, genetic interrelationships, and stratigraphy over the continuum of
847 fluvial channel-form bounding surfaces: An illustration from middle Cretaceous strata,
848 Southeastern Colorado: Sedimentary Geology, v. 144, nos. 3–4, p. 179–222.
849 Holbrook, J., and Wanas, H., 2014, A fulcrum approach to assessing source-to-sink mass balance
850 using channel paleohydrologic paramaters derivable from common fluvial data sets with an
851 example from the cretaceous of Egypt: Journal of Sedimentary Research, v. 84, no. 5, p. 349–
852 372.
853 Holbrook, J.M., 1996, Complex fluvial response to low gradients at maximum regression: A
854 genetic link between smooth sequence-boundary morphology and architecture of overlying
855 sheet sandstone: Journal of Sedimentary Research, v. 66, no. 4, p. 713–722.
856 Jablonski, B.V.J., and Dalrymple, R.W., 2016, Recognition of strong seasonality and climatic
857 cyclicity in an ancient, fluvially dominated, tidally influenced point bar: Middle McMurray
858 Formation, Lower Steepbank River, north-eastern Alberta, Canada: Sedimentology, v. 63, no.
859 3, p. 552–585.
860 Jacobsen, R.E., and Burr, D.M., 2016, Greater contrast in Martian hydrological history from more
861 accurate estimates of paleodischarge: Geophysical Research Letters, v. 43, no. 17, p. 8903–
862 8911.
863 Kästner, K., Hoitink, A.J.F., Vermeulen, B., Geertsema, T.J., and Ningsih, N.S., 2017, Distributary
864 channels in the fluvial to tidal transition zone: Journal of Geophysical Research: Earth
865 Surface, v. 122, no. 3, p. 696–710.
866 Korus, J.T., and Fielding, C.R., 2015, Asymmetry in Holocene river deltas: Patterns, controls, and
867 stratigraphic effects: Earth-Science Reviews, v. 150, p. 219–242.

868 Kravtsova, V.I., Mikhailov, V.N., and Kidyaeva, V.M., 2009, Hydrological regime, morphological
869 features and natural territorial complexes of the Irrawaddy River Delta (Myanmar): Water
870 Resources, v. 36, no. 3, p. 243–260.
871 Lamb, M.P., Nittrouer, J.A., Mohrig, D., and Shaw, J., 2012, Backwater and river plume controls
872 on scour upstream of river mouths: Implications for fluvio-deltaic morphodynamics: J.
873 Geophys. Res, v. 117, p. 1002.
874 Leclair, S.F., and Bridge, J.S., 2001, Quantitative interpretation of sedimentary structures formed
875 by river dunes: Journal of Sedimentary Research, v. 71, no. 5, p. 713–716.
876 Leopold, L.B., and Maddock, T., 1953, The Hydraulic Geometry of Stream Channels and Some
877 Physiographic Implications:, accessed December 29, 2020, at Professional Paper.
878 Li, W., Bhattacharya, J.P., and Wang, Y., 2011, Delta asymmetry: Concepts, characteristics, and
879 depositional models: Petroleum Science, v. 8, no. 3, p. 278–289.
880 Lin, W., and Bhattacharya, J.P., 2017, Estimation of source-to-sink mass balance by a fulcrum
881 approach using channel paleohydrologic parameters of the cretaceous dunvegan formation,
882 Canada: Journal of Sedimentary Research, v. 87, no. 1, p. 97–116.
883 Lin, W., and Bhattacharya, J.P., 2021, Storm-flood-dominated delta: A new type of delta in stormy
884 oceans: Sedimentology, v. 68, no. 3, p. 1109–1136.
885 Lyster, S.J., Whittaker, A.C., Allison, P.A., Lunt, D.J., and Farnsworth, A., 2020, Predicting
886 sediment discharges and erosion rates in deep time—examples from the late Cretaceous North
887 American continent: Basin Research, v. 32, no. 6, p. 1547–1573.
888 Lyster, S.J., Whittaker, A.C., Hampson, G.J., Hajek, E.A., Allison, P.A., and Lathrop, B.A., 2021,
889 Reconstructing the morphologies and hydrodynamics of ancient rivers from source to sink:
890 Cretaceous Western Interior Basin, Utah, USA: Sedimentology.

Martin, J., Fernandes, A.M., Pickering, J., Howes, N., Mann, S., and McNeil, K., 2018, The Stratigraphically Preserved Signature of Persistent Backwater Dynamics in a Large Paleodelta System: The Mungaroo Formation, North West Shelf, Australia: Journal of Sedimentary Research, v. 88, no. 7, p. 850–872.

Merritt, D.M., and Wohl, E.E., 2003, Downstream hydraulic geometry and channel adjustment during a flood along an ephemeral, arid-region drainage: Geomorphology, v. 52, nos. 3–4, p. 165–180.

Montgomery, D.R., and Gran, K.B., 2001, Downstream variations in the width of bedrock channels: Water Resources Research, v. 37, no. 6, p. 1841–1846.

Morgan, A.M., and Craddock, R.A., 2019, Assessing the Accuracy of Paleodischarge Estimates for Rivers on Mars: Geophysical Research Letters, v. 46, no. 21, p. 11738–11746.

Nienhuis, J.H., Ashton, A.D., Edmonds, D.A., Hoitink, A.J.F., Kettner, A.J., Rowland, J.C., and Törnqvist, T.E., 2020, Global-scale human impact on delta morphology has led to net land area gain: Nature, v. 577, no. 7791, p. 514–518.

Nittrouer, J.A., 2013, Backwater hydrodynamics and sediment transport in the lowermost Mississippi River delta: Implications for the development of fluvial-deltaic landforms in a large lowland river, in IAHS ed., Proceedings of HP1, IAHS-IAPSO-IASPEI Assembly, Gothenburg, Sweden, July 2013 (IAHS Publ. 358, 2013).: Gothenburg, IAHS Publication.

Oboh-Ikuenobe, F., Holbrook, J., Scott, R., Akins, S., Evetts, M., Benson, D., and Pratt, L., 2008, Anatomy of Epicontinental Flooding: Late Albian-Early Cenomanian of the Southern U.S. Western Interior Basin: Special Paper - Geological Association of Canada, no. 48.

Olariu, C., and Bhattacharya, J.P., 2006, Terminal distributary channels and delta front architecture of river-dominated delta systems: Journal of Sedimentary Research, v. 76, no. 2, p. 212–233.

914 Paola, C., and Mohrig, D., 1996, Palaeohydraulics revisited: palaeoslope estimation in coarse-
915 grained braided rivers: Basin Research, v. 8, no. 3, p. 243–254.
916 Parker, G., 1978, Self-formed straight rivers with equilibrium banks and mobile bed. Part 2. The
917 gravel river: Journal of Fluid Mechanics, v. 89, no. 1, p. 127–146.
918 Parker, G., 2004, E-book: 1D Sediment Transport Morphodynamics with Applications to Rivers
919 and Turbidity Currents:
920 Parker, G., Wilcock, P.R., Paola, C., Dietrich, W.E., and Pitlick, J., 2007, Physical basis for quasi-
921 universal relations describing bankfull hydraulic geometry of single-thread gravel bed rivers:
922 Journal of Geophysical Research: Earth Surface, v. 112, no. 4.
923 Pecha, M.E., Gehrels, G.E., Karlstrom, K.E., Dickinson, W.R., Donahue, M.S., Gonzales, D.A.,
924 and Blum, M.D., 2018, Provenance of Cretaceous through Eocene strata of the Four Corners
925 region: Insights from detrital zircons in the San Juan Basin, New Mexico and Colorado:
926 Geosphere, v. 14, no. 2, p. 785–811.
927 Pettit, B.S., Blum, M., Pecha, M., McLean, N., Bartschi, N.C., and Saylo, J.E., 2019, Detrital-
928 Zircon U-Pb Paleodrainage Reconstruction and Geochronology of the Campanian
929 Blackhawk–Castlegate Succession, Wasatch Plateau and Book Cliffs, Utah, U.S.A.: Journal
930 of Sedimentary Research, v. 89, no. 4, p. 273–292.
931 Prasojo, O.A., Hoey, T.B., Owen, A., and Williams, R.D., 2022, Slope break and avulsion
932 locations scale consistently in global deltas: Geophysical Research Letters, p.
933 e2021GL093656.
934 Prasojo, O.A., Hoey, T.B., Owen, A., and Williams, R.D., 2023, Down-delta hydraulic geometry
935 and its application to the rock record: Sedimentology.

936 Rice, S., and Church, M., 1996, Sampling surficial fluvial gravels; the precision of size distribution
937 percentile sediments: Journal of Sedimentary Research, v. 66, no. 3, p. 654–665.
938 de Rose, R.C., Stewardson, M.J., and Harman, C., 2008, Downstream hydraulic geometry of rivers
939 in Victoria, Australia: Geomorphology, v. 99, nos. 1–4, p. 302–316.
940 Sassi, M.G., Hoitink, A.J.F., de Brye, B., and Deleersnijder, E., 2012, Downstream hydraulic
941 geometry of a tidally influenced river delta: Journal of Geophysical Research: Earth Surface,
942 v. 117, no. F4, p. n/a-n/a.
943 Scott R.W., Holbrook J.M., Oboh-Ikuenobe F.E., Evetts M.J., Benson D.G., and Kues B.S., 2004,
944 Middle Cretaceous Stratigraphy, Southern Western Interior Seaway, New Mexico and
945 Oklahoma: The Mountain Geologist.
946 Sharma, S., Bhattacharya, J.P., and Richards, B., 2017, Source-to-sink sediment budget analysis
947 of the Cretaceous Ferron Sandstone, Utah, U.S.A, using the fulcrum approach: Journal of
948 Sedimentary Research, v. 87, no. 6, p. 594–608.
949 Sharman, G.R., Sylvester, Z., and Covault, J.A., 2019, Conversion of tectonic and climatic forcings
950 into records of sediment supply and provenance: Scientific Reports 2019 9:1, v. 9, no. 1, p.
951 1–7.
952 Swenson, J.B., 2005, Relative importance of fluvial input and wave energy in controlling the
953 timescale for distributary-channel avulsion: Geophysical Research Letters, v. 32, no. 23, p.
954 1–5.
955 Syvitski, J.P.M., and Milliman, J.D., 2007, Geology, Geography, and Humans Battle for
956 Dominance over the Delivery of Fluvial Sediment to the Coastal Ocean: The Journal of
957 Geology, v. 115, p. 1–19.

Trampush, S.M., Huzurbazar, S., and McElroy, B., 2014, Empirical assessment of theory for bankfull characteristics of alluvial channels: Water Resources Research, v. 50, no. 12, p. 9211–9220.

Vakarelov, B.K., and Ainsworth, R.B., 2013, A hierarchical approach to architectural classification in marginal-marine systems: Bridging the gap between sedimentology and sequence stratigraphy: AAPG Bulletin, v. 97, no. 7, p. 1121–1161.

Whittaker, A.C., 2012, How do landscapes record tectonics and climate? Lithosphere, v. 4, no. 2, p. 160–164.

Whittaker, A.C., Duller, R.A., Springett, J., Smithells, R.A., Whitchurch, A.L., and Allen, P.A., 2011, Decoding downstream trends in stratigraphic grain size as a function of tectonic subsidence and sediment supply: Bulletin of the Geological Society of America, v. 123, nos. 7–8, p. 1363–1382.

Wohl, E., and David, G.C.L., 2008, Consistency of scaling relations among bedrock and alluvial channels: Journal of Geophysical Research, v. 113, no. F4, p. F04013.

van Yperen, A.E., Holbrook, J.M., Poyatos-Moré, M., and Midtkandal, I., 2019, Coalesced delta-front sheet-like sandstone bodies from highly avulsive distributary channels: The low-accommodation mesa rica sandstone (Dakota Group, New Mexico, USA): Journal of Sedimentary Research, v. 89, no. 7, p. 654–678.

van Yperen, A.E., Holbrook, J.M., Poyatos-Moré, M., Myers, C., and Midtkandal, I., 2021, Low-accommodation and backwater effects on sequence stratigraphic surfaces and depositional architecture of fluvio-deltaic settings (Cretaceous Mesa Rica Sandstone, Dakota Group, USA): Basin Research, v. 33, no. 1, p. 513–543.

FIGURE CAPTIONS

Figure 1. Landsat 5 images (all around year 2000) from: A. tide-influenced, river-dominated Mahakam delta, Indonesia; B. wave-influenced Baram delta, Malaysia; tide-dominated C. tide-dominated Fly delta, Papua New Guinea and D. river-dominated Pahang delta, Malaysia. Changes in channel width away from the distal limits, which are plotted in the lower panels. Differences in morphological patterns depend on the interaction between dynamic catchment (water and sediment inputs) and marine (wave energy, tidal energy) variables that interact to produce delta morphology.

Figure 2. A: Distribution of river deltas studied. B: The semicircular grid is used to determine measurement locations for distributary channels widths. C: Enlarged version of the measured channel width from Fig. 2B. Channel widths were made at the red lines which are perpendicular to the banks of the wetted distributary channels. Inset shows measurement method when mid-channel bars are present. The spacing of the semicircular grid is defined as ~10 times the channel width at the apex of the delta (W_A).

Figure 3. Paleogeographic reconstruction of the Cretaceous lower Mesa Rica fluvio-deltaic depositional system (modified from Van Yperen et al., 2019). Due to the scale of the figure, not all 13 data points are shown. See Table 2 for locations of all channel width measurements.

Figure 4. A-C: Distribution of dimensionless measured channel widths from (A) river-, (B) tide- and, (C) wave-dominated deltas. *p*-values are from the non-parametric Kruskal-Wallis one-way analysis of variance test comparing the distributions of channel width at different locations along the delta. D-E: examples of (D) river- and (E) tide-dominated deltas, with the upstream-

downstream boundary positions inferred from the changes of channel width on (A) and (B). F: Map view the Paraibo do Sul delta in Brazil showing differences in updrift and downdrift characteristics of a wave-dominated delta (modified from Li et al., 2011). G: Map view and cross-section view of a mouth bar. Boxes on D depict the location of the mouth bars shown in G. Color gradients show the contrast between upstream and downstream parts of the delta plains.

Figure 5. Mean standard error of dimensionless channel width (S_{W^*}) versus number of measurements (N) from the upstream and downstream parts of river- (A,B, respectively) and tide-dominated (C,D) deltas. E: Mean standard error versus N from wave-dominated deltas. F-K: Percentile standard errors of the dimensionless widths for the selected B values from plots (A-E). B indicates the number of repetitions in the bootstrap calculations. Inset plots (A-E) show greater detail for low N. The dark orange lines show the number of repetitions (B) that produced the most stable, generally monotonic relationships between standard error of dimensionless width and number of measurements.

Figure 6. A-E: Scaling relationships between bankfull discharge (Q_2) and median channel widths (W_{med}) for river-, tide-, wave-dominated deltas. (F) Scaling relationship between bankfull discharge (Q_2) and individual channel widths (W) for the full dataset. (A) and (C) are for upstream parts of river- and tide-dominated deltas, and (B) and (D) are for their downstream parts, respectively. Ordinary least squares regression lines and 95% confidence intervals (shaded areas) shown; R^2 = coefficient of determination of the scaling relationship, p = statistical significance, and s = standard error of residuals. Note that number of samples is smaller on this figure due to incomplete bankfull discharge dataset.

Figure 7. A: Distribution of 13 measured channel widths from the lower Mesa Rica, grouped by geographical zone across the delta plain. B: Density plot of the 13 measured channel widths: whole population (dark yellow); transitional zone (grey); and, distal zone (dark blue). Median, mean, and mode values (continuous, dashed and dotted vertical lines, respectively) are calculated from the combined transitional and distal data (N=12), excluding the single width measurement from the proximal zone. C: Standard error of dimensionless width (S_{W*}) versus number of samples (N) of the 12 measured channel widths from the lower Mesa Rica.

TABLE CAPTIONS

Table 1. Summary of global and climate-classified scaling relationships between water discharge and distributary channel widths from Prasojo et al. (2023). W_{med} refers to the median value of measured channel widths and Q_2 is 2-year flood recurrence interval that is assumed to be the bankfull discharge.

Table 2. Distribution of the 13 measured channel widths from the lower Mesa Rica along with the zonation and latitude-longitude positions.

Figure 1

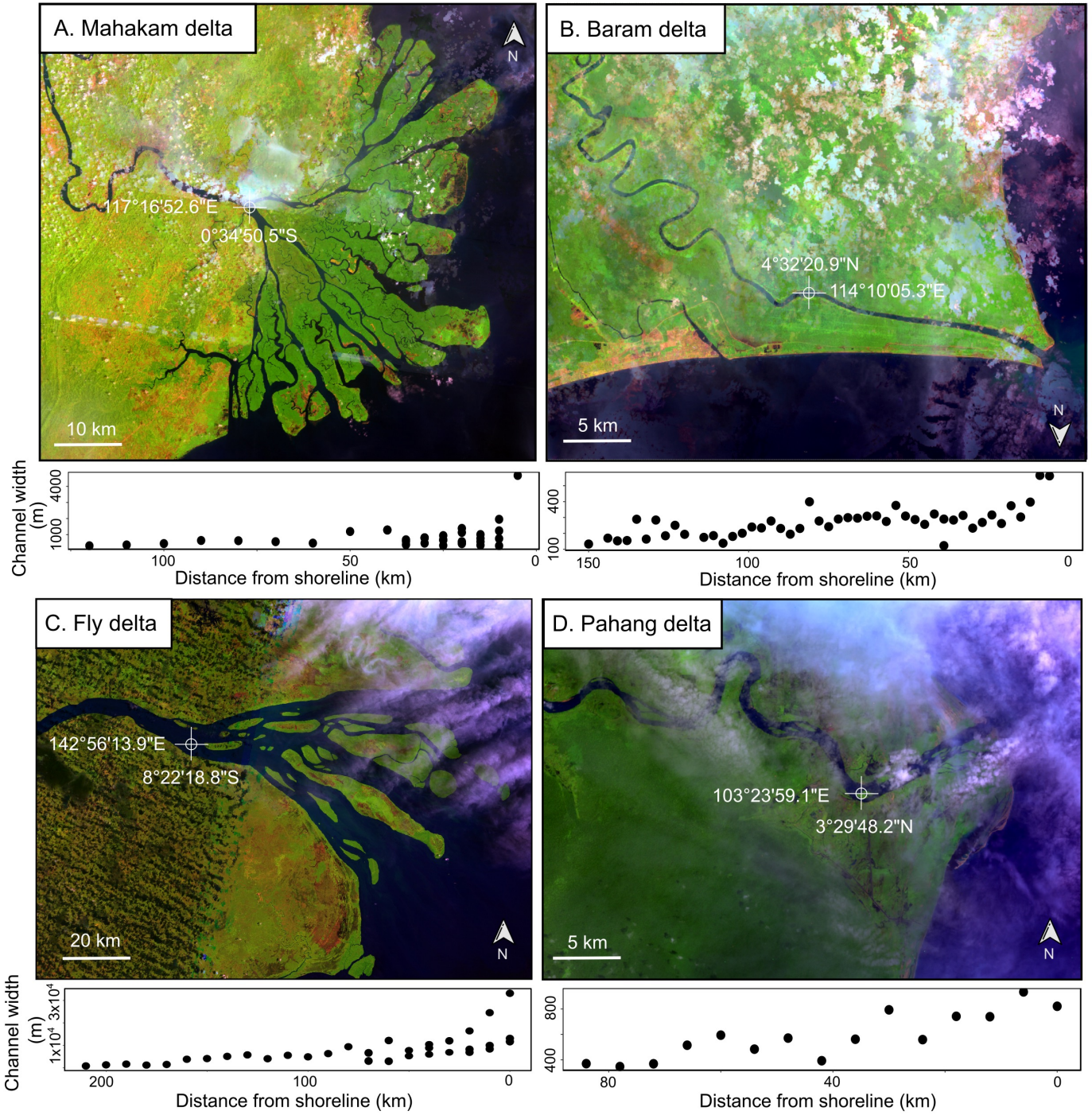
A. Mahakam delta
117°16'52.6"E
0°34'50.5"S
10 km
N
B. Baram delta
4°32'20.9"N
114°10'05.3"E
5 km
N
Channel width (m)
4000
1000
100
50
0
Distance from shoreline (km)
400
100
150
100
50
0
Distance from shoreline (km)
C. Fly delta
142°56'13.9"E
8°22'18.8"S
20 km
N
D. Pahang delta
103°23'59.1"E
3°29'48.2"N
5 km
N
Channel width (m)
1x10^4
3x10^4
200
100
0
Distance from shoreline (km)
800
400
80
40
0
Distance from shoreline (km)

Figure 2

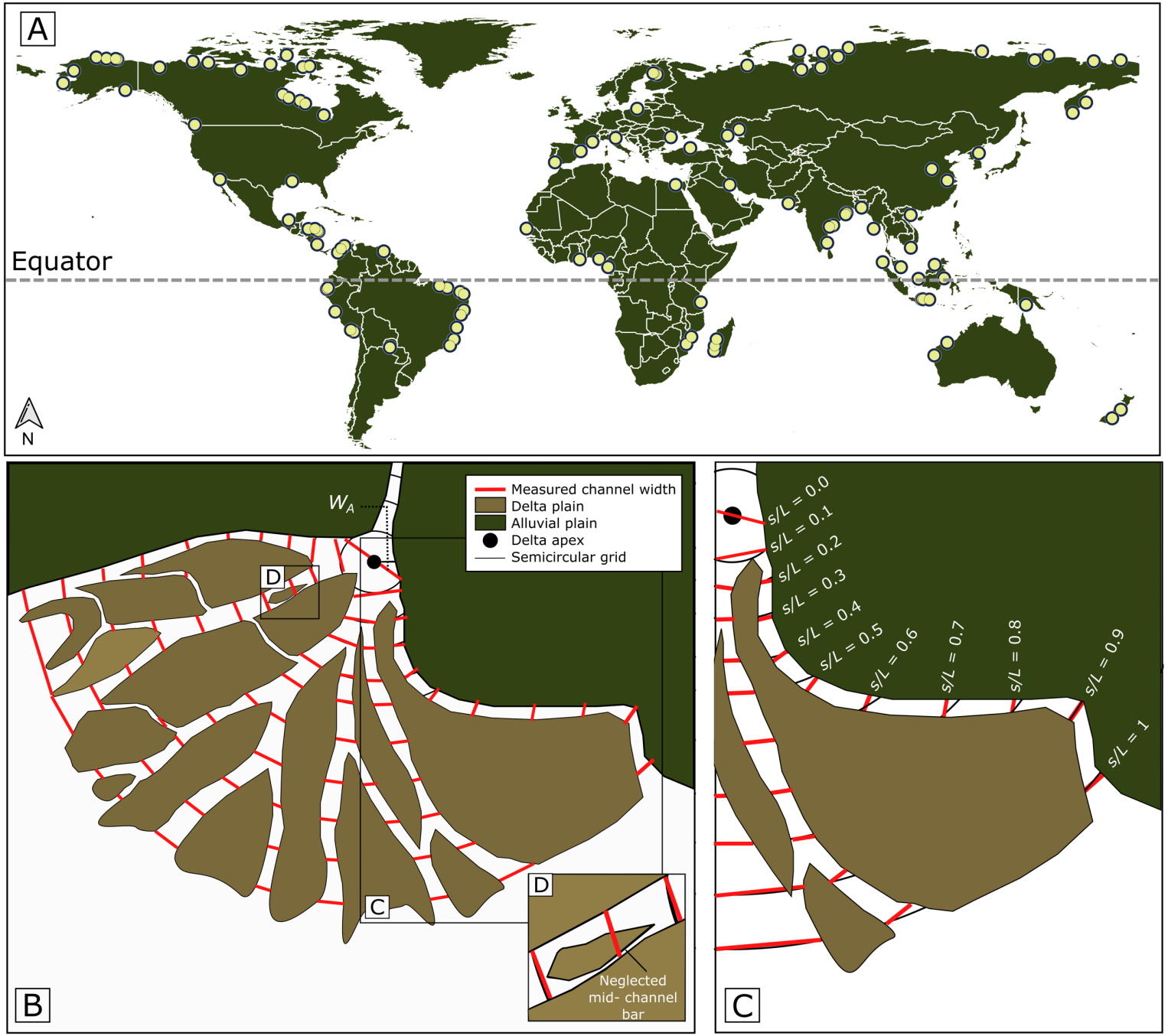
A
Equator
N
B
W_A
Measured channel width
Delta plain
Alluvial plain
Delta apex
Semicircular grid
D
C
D
Neglected mid- channel bar
C
s/L = 0.0
s/L = 0.1
s/L = 0.2
s/L = 0.3
s/L = 0.4
s/L = 0.5
s/L = 0.6
s/L = 0.7
s/L = 0.8
s/L = 0.9
s/L = 1

Figure 3

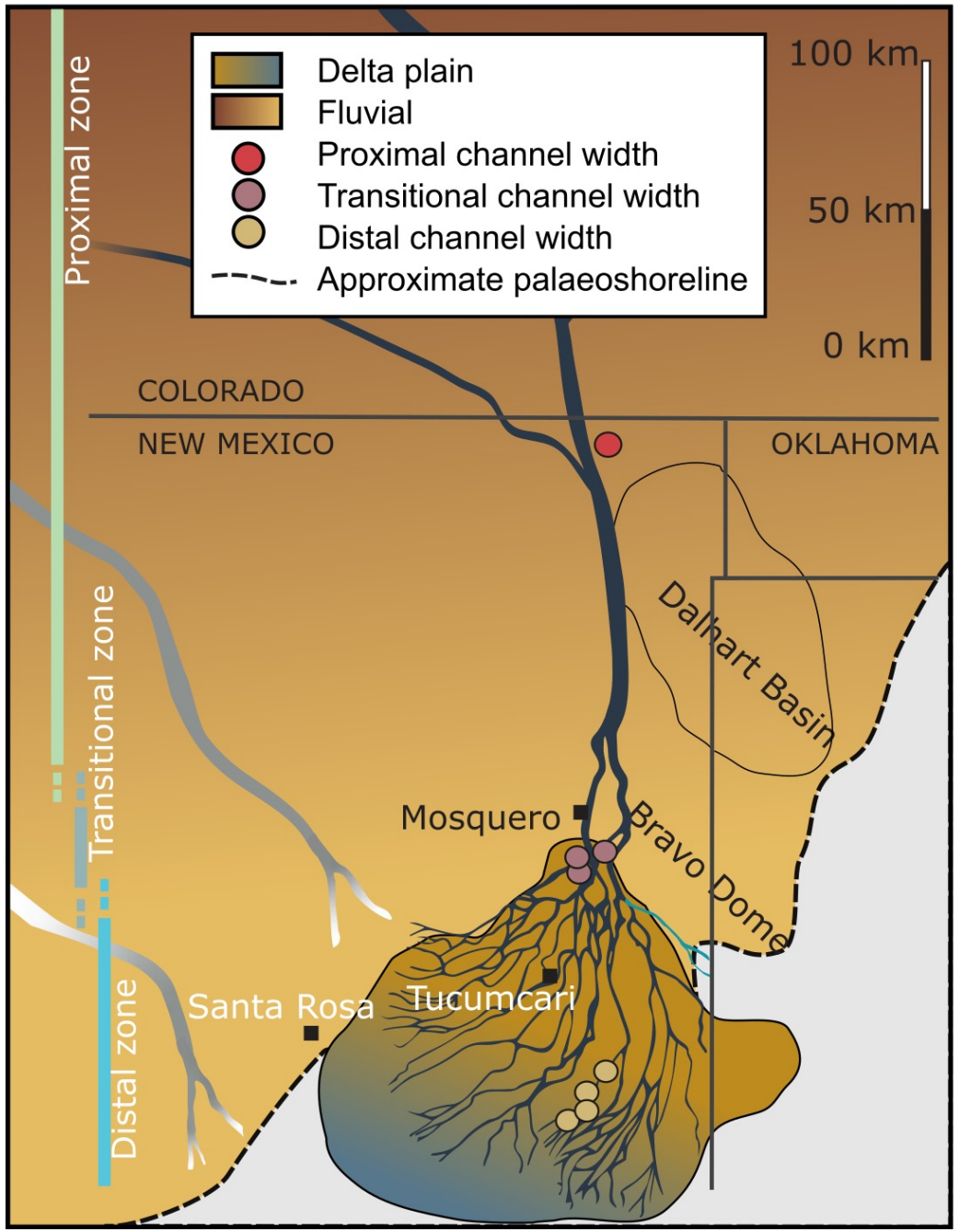
Delta plain
Fluvial
Proximal channel width
Transitional channel width
Distal channel width
Approximate palaeoshoreline
100 km
50 km
0 km
Proximal zone
Transitional zone
Distal zone
COLORADO
NEW MEXICO
OKLAHOMA
Dalhart Basin
Bravo Dome
Mosquero
Tucumcari
Santa Rosa

Figure 4

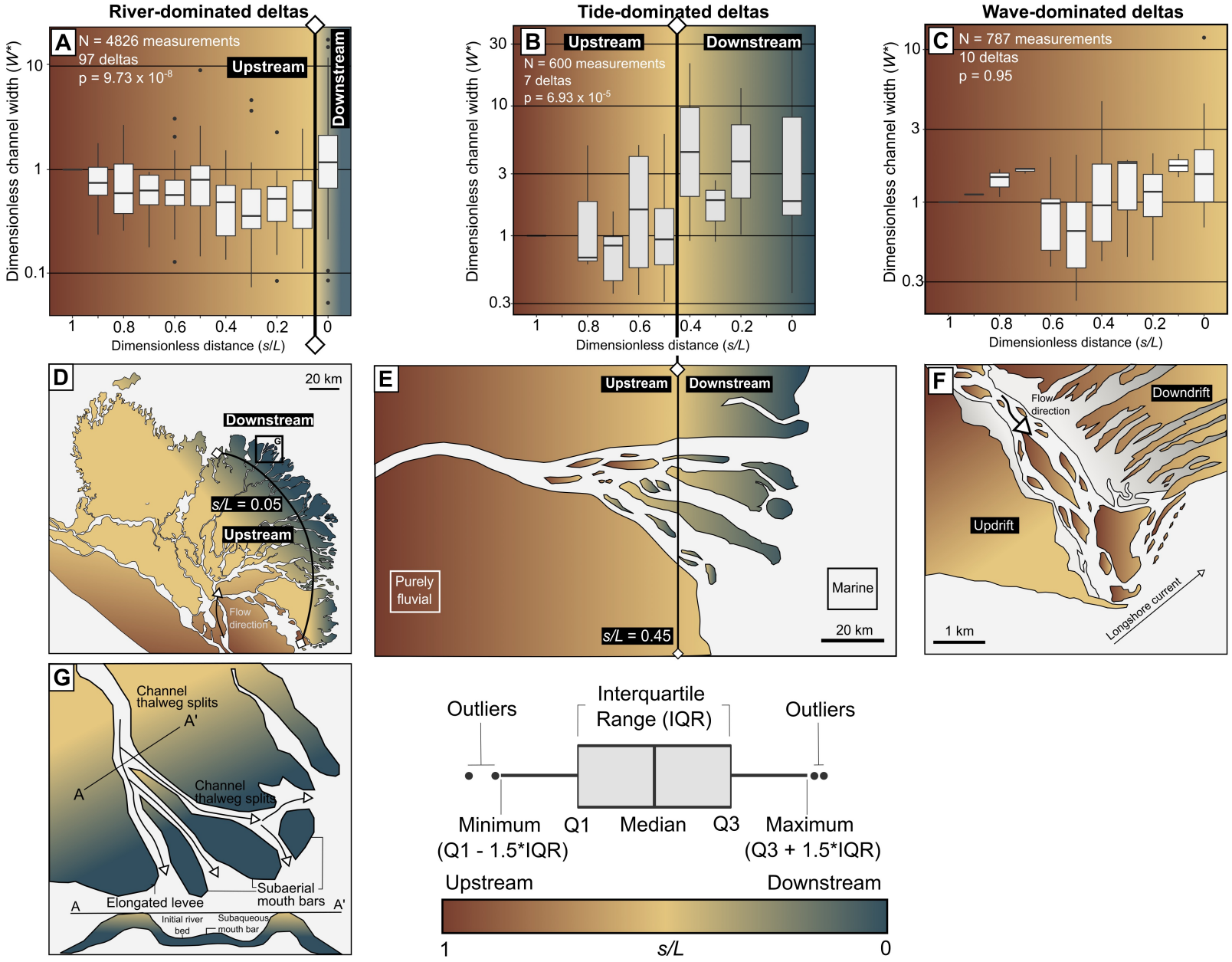
River-dominated deltas
Tide-dominated deltas
Wave-dominated deltas
A
N = 4826 measurements
97 deltas
p = 9.73 x 10-8
Upstream
Downstream
Dimensionless channel width (W*)
Dimensionless distance (s/L)
B
Upstream
Downstream
N = 600 measurements
7 deltas
p = 6.93 x 10-5
C
N = 787 measurements
10 deltas
p = 0.95
D
20 km
Downstream
s/L = 0.05
Upstream
Flow direction
E
Upstream
Downstream
Purely fluvial
Marine
s/L = 0.45
20 km
F
Flow direction
Downdrift
Updrift
Longshore current
1 km
G
Channel thalweg splits
A'
A
Channel thalweg splits
Subaerial mouth bars
Elongated levee
Initial river bed
Subaqueous mouth bar
Outliers
Interquartile Range (IQR)
Outliers
Minimum (Q1 - 1.5*IQR)
Q1
Median
Q3
Maximum (Q3 + 1.5*IQR)
Upstream
Downstream
s/L

Figure 5

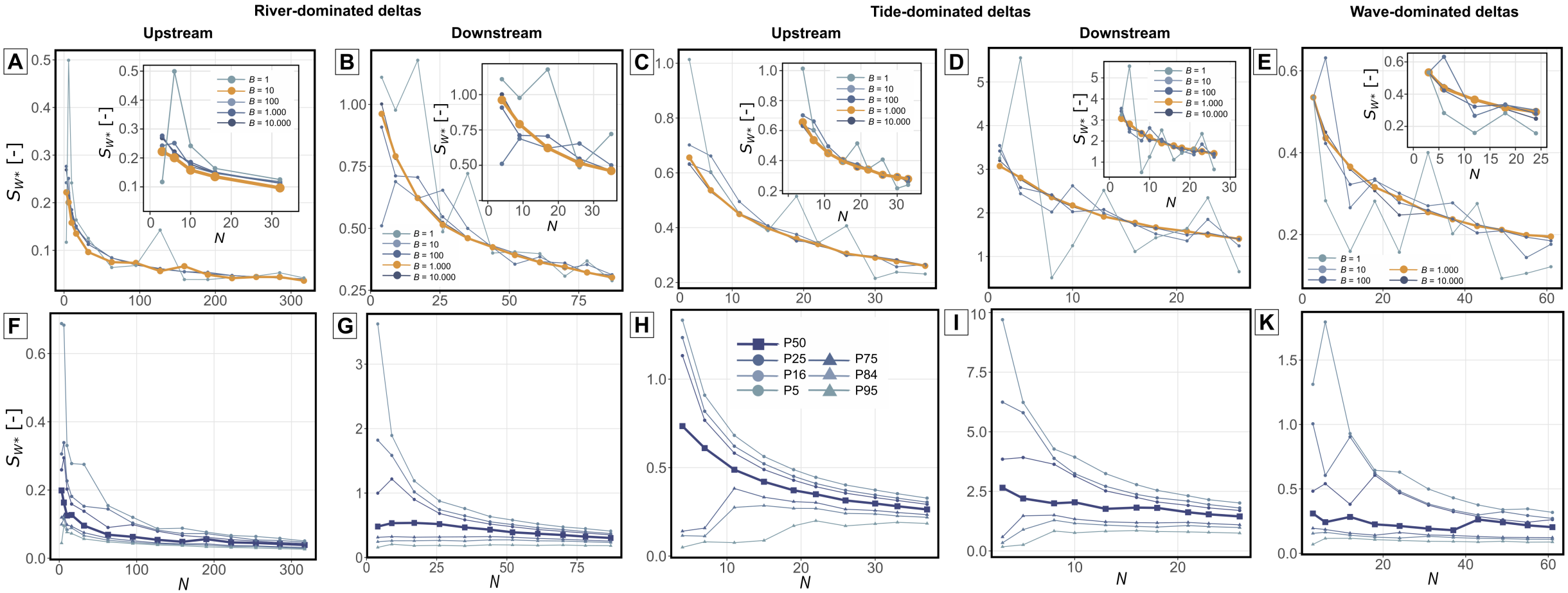
River-dominated deltas
Tide-dominated deltas
Wave-dominated deltas
Upstream
Downstream
Upstream
Downstream
A
B
C
D
E
F
G
H
I
K
S_{W^*} [-]
N
B = 1
B = 10
B = 100
B = 1.000
B = 10.000
P50
P25
P16
P5
P75
P84
P95

Figure 6

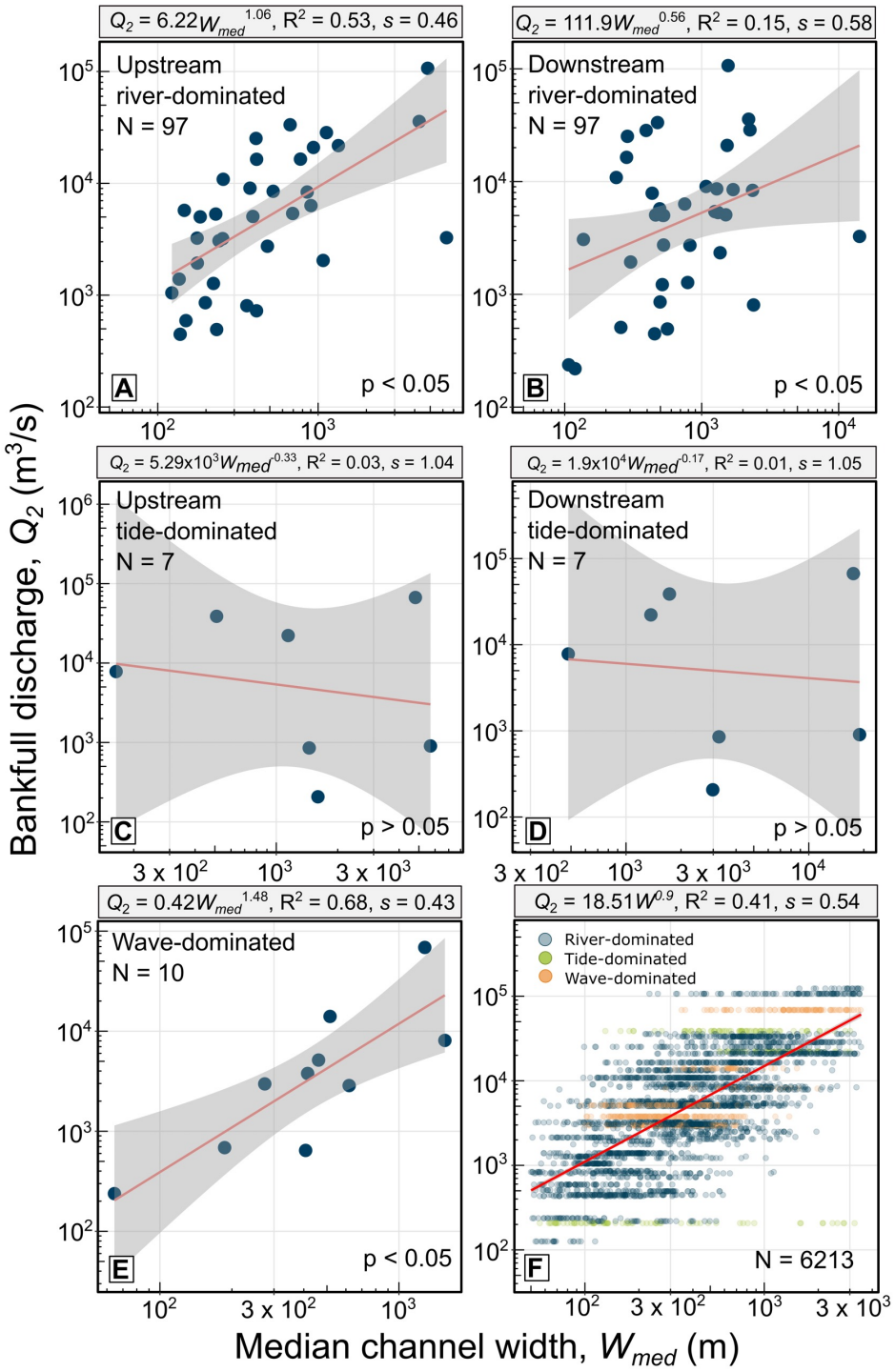
$Q_2 = 6.22W_{med}^{1.06}$, $R^2 = 0.53$, $s = 0.46$
Upstream
river-dominated
N = 97
A
p < 0.05
$Q_2 = 111.9W_{med}^{0.56}$, $R^2 = 0.15$, $s = 0.58$
Downstream
river-dominated
N = 97
B
p < 0.05
$Q_2 = 5.29x10^3W_{med}^{0.33}$, $R^2 = 0.03$, $s = 1.04$
Upstream
tide-dominated
N = 7
C
p > 0.05
$Q_2 = 1.9x10^4W_{med}^{0.17}$, $R^2 = 0.01$, $s = 1.05$
Downstream
tide-dominated
N = 7
D
p > 0.05
$Q_2 = 0.42W_{med}^{1.48}$, $R^2 = 0.68$, $s = 0.43$
Wave-dominated
N = 10
E
p < 0.05
$Q_2 = 18.51W^{0.9}$, $R^2 = 0.41$, $s = 0.54$
River-dominated
Tide-dominated
Wave-dominated
F
N = 6213
Bankfull discharge, Q_2 (m^3/s)
Median channel width, W_{med} (m)

Figure 7

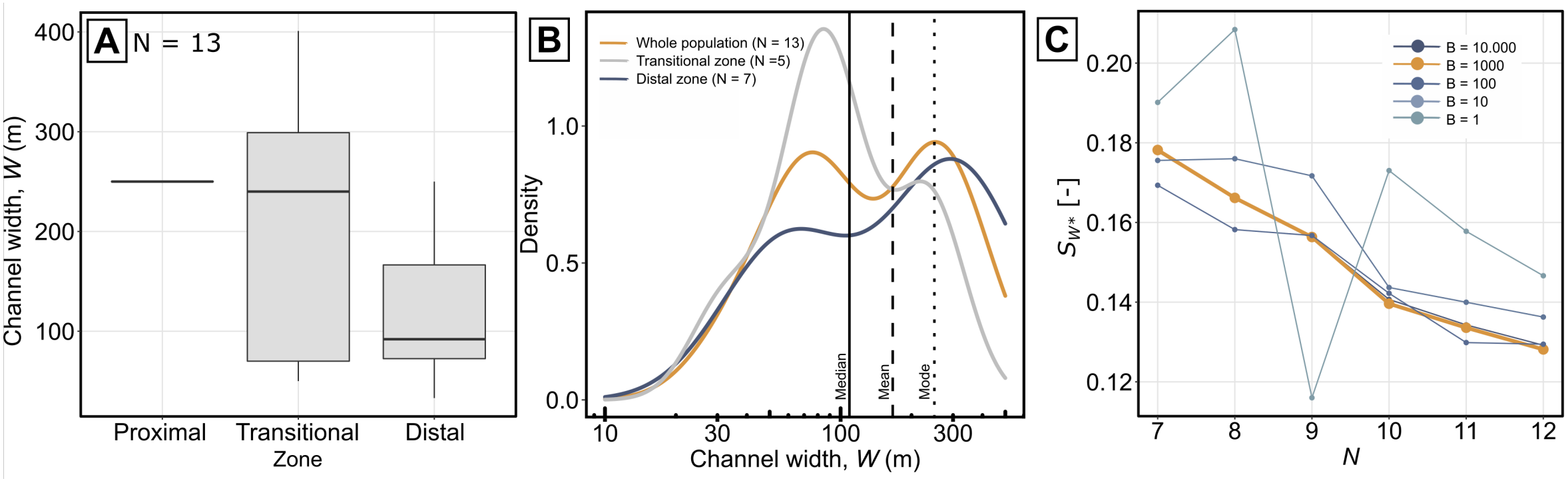
A
N = 13
Channel width, W (m)
400
300
200
100
Proximal
Transitional
Distal
Zone
B
Whole population (N = 13)
Transitional zone (N =5)
Distal zone (N = 7)
Density
1.0
0.5
0.0
Median
Mean
Mode
10
30
100
300
Channel width, W (m)
C
B = 10.000
B = 1000
B = 100
B = 10
B = 1
S_{W^*} [-]
0.20
0.18
0.16
0.14
0.12
7
8
9
10
11
12
N

Table 1. Summary of global and climate-classified scaling relationships between water discharge and distributary channel widths from Prasojo et al., 2023. W_{med} refers to the median value of measured channel widths and Q_2 is 2-year flood recurrence interval that is assumed to be the bankfull discharge.

Classification	N	Equation	Statistical significance
Global	66	$Q_2 = 0.34 W_{med}^{1.48}$	$R^2 = 0.77$; $p = 2.2 \times 10^{-16}$
Arid	11	$Q_2 = 0.04 W_{med}^{1.67}$	$R^2 = 0.52$; $p = 1.2 \times 10^{-2}$
Cold	14	$Q_2 = 0.01 W_{med}^{1.65}$	$R^2 = 0.94$; $p = 1.07 \times 10^{-8}$
Polar	6	$Q_2 = 0.12 W_{med}^{1.55}$	$R^2 = 0.91$; $p = 3.09 \times 10^{-3}$
Temperate	8	$Q_2 = 0.07 W_{med}^{1.66}$	$R^2 = 0.88$; $p = 5.6 \times 10^{-4}$
Tropical	27	$Q_2 = W_{med}^{1.4}$	$R^2 = 0.63$; $p = 1.5 \times 10^{-6}$

Table 2. Distribution of the 13 measured channel widths from the lower Mesa Rica along with the zonation and latitude-longitude positions.

Measured width (m)	Zone	Latitude	Longitude
250	Proximal	36.93349	-103.62979
401	Transitional	35.49859	-103.81257
299	Transitional	35.53891	-103.84624
240	Transitional	35.53491	-103.86028
70	Transitional	35.54482	-103.84091
50	Transitional	35.53751	-103.84859
71	Distal	34.991298	-103.396205
92	Distal	34.991222	-103.41928
109	Distal	34.91677	-103.49411
33	Distal	34.86206	-103.54559
224	Distal	34.937565	-103.469176
74	Distal	34.93272	-103.48047
250	Distal	34.99736	-103.38935